CHALMERS

Preparation and Characterization of Novel Microcapsules

Master of Science Thesis in the Master Degree Program Material and Nanotechnology

ADELE KHAVARI

Department of Chemical and Biological Engineering
Division of Applied Chemistry
CHALMERS UNIVERSITY OF TECHNOLOGY
Göteborg, Sweden, 2010

Preparation and Characterization of Novel Microcapsules

Master of Science Thesis in the Master Degree Program Material and Nanotechnology

Adele Khavari

Supervisors: Professor Jan-Erik Löfroth & Professor Magnus Nydén
Examiner: Professor Krister Holmberg

Department of Chemical and Biological Engineering
CHALMERS UNIVERSITY OF TECHNOLOGY
Göteborg, Sweden 2010

Preparation and Characterization of Novel Microcapsules

Department of Chemical and Biological Engineering
Chalmers University of Technology
SE-412 96 Göteborg
Sweden

Telephone + 46 (0)31-772 1000

Department of Chemical and Biological Engineering
Göteborg, Sweden 2010

Abstract

The aim of this project has been to produce core-shell particles containing oil as the core, and water-insoluble polymers as the shell. Since the particles were to be used in experiments with light scattering (LS) and nuclear magnetic resonance diffusometry (NMRd) for probing the structure of hydrogels following particle diffusion in the gel systems, the size of the particles was intended to be below 1 μm and detectable with NMR.

Oil-containing microparticles were produced by solvent evaporation protocols using a homogenizer or a microfluidizer. Different types of fluorinated oils were encapsulated to give core-shell particles ranging in size from about 1 μm to 150 nm with a polydispersity ranging from 0.1 to 0.4 in terms of the relative standard deviation of the size distributions as determined by dynamic light scattering.

Further, static light scattering (SLS) was used to obtain experimental form factors of the particles to be compared with theoretical ones. Successful data analysis could then have given information about, e.g. shell thickness of the particles, size of the core, and average density of the particles.

However, it was found that it was not possible to describe the particles as classical core-shell particles from these light scattering experiments. The experimental form factors deviated substantially from what could be theoretically simulated.

The explanation for this could tentatively be based on results from experiments with the technique QCM-D (quartz crystal microbalance with dissipation monitoring). It was found that the emulsifier used to produce the particles seemed to bind irreversibly to the shell polymer, creating a thick layer around the particles. Thus, the simple core-shell model used to analyze the SLS data was probably wrong.

Future possible work is outlined in this Thesis, emphasizing the need for better control of some parameters crucial for forming the core-shell particles, e.g. temperature and stirring speeds. Also, the characterization of such complex particles with an adsorbed polymer layer would probably be more accurate if scattering techniques based on neutrons and X-rays were used. Alternatively, a more complicated theoretical model for the form factor might be necessary for successful LS data analysis.

Contents

1 INTRODUCTION

Encapsulation of different molecules in so called microcapsules is of major importance in many industrial applications. By definition a microcapsule is a particle with a core and shell structure where the core can be a solid, liquid, or gas system and the shell can be a polymer system or an inorganic material.[1]

Microcapsules are widely used in applications in which an active compound needs to be protected from the environmental conditions (UV, oxygen, and moisture) either to avoid the side effect of the active or to prolong the storage life time of the active. Other applications are when controlled release, or prevented chemical reaction between the active and surrounding is required. For example, controlled release of an active medical agent can be a mean to make available the drug during a long time to achieve, e.g. a once-daily dosing of the medicine.[2] The same principle can be used in agricultural and paint applications, where now, however, the release of, e.g. a pesticide might be necessary to prolong for months.[2] Microcapsules can also be used to mask bitter taste of active substance in food and pharmaceutical products.[3]

There are different techniques for the production of microcapsules, such as phase separation, spray-drying, interfacial and in-situ polymerization, and solvent evaporation. Phase separation[4] is a method in which core material is suspended into a solution of shell materials and where the phase separation is induced by different techniques like adding non solvent. This technique is, however, not suitable for production of particles in the micrometer scale. Spray drying[4] is a quite simple technique but not suitable for highly temperature sensitive material. Moreover, particle size control is not easy with this technique, Polymerization[4] is a method which is principally based on interfacial polymerization. In this method polymerization occurs at the interface between the aqueous phase and the emulsion droplet. When the polymer film is formed, the active is encapsulated.

The technique mostly used is however the solvent evaporation technique,[4,5] since it does not require, e.g. elevated temperature and gives the possibility to control the size of the produced particles in the range of nano- to micrometer. In this technique both core and shell material are dissolved in a good solvent and emulsified in an aqueous phase in the presence of an emulsifier soluble in the aqueous phase. Finally, the solvent for the core and shell materials is evaporated at, e g, room temperature.

Apart from the industrial applications mentioned above, core-shell particles can be used as so called probe-particles, i.e. particles incorporated in a material and that can be detected by some technique to get information about material properties. Incorporation of particles with suitable properties in, e.g., a hydrogel will make it possible to follow the transport and movement of the particles in the material, reflecting the structure of the material and its dynamics. Depending on the detection technique to be used, the properties of the particles are crucial.

Some of the work at the Division of Applied Chemistry at Chalmers is focused on hydrogel properties. A hydrogel is a polymer system based on, e.g. biopolymers like

alginate, agarose, gellan gum, carrageenan, etc, or synthetic polymers like polyacrylic acid, that can form gel-like systems built up by physical or chemical crosslinks. Such systems can hold up to more than 99% w/w of water when swelled in water and are frequently found in several industrial products within the food, pharmaceutics, paint etc. industry. The work at the division is carried out within the VINNOVA competence centre SUMO (Supramolecular biomaterials) and several different techniques are used to study material properties, e.g. NMR (nuclear magnetic resonance), LS (light scattering), and FRAP (fluorescence recovery after photobleaching), each of these techniques putting different demands on the particle to be used.

One way to get a signal suitable for NMR would be to incorporate fluorinated oil in the core of a core-shell particle. The requirement then is low solubility of the oil in the water, so that no release to the aqueous environment of the particles is obtained when a hydrogel is loaded with the particles. For FRAP, such particles must have a fluorescent molecule, preferably at their surface. LS requires rather monodisperse particles to better understand obtained results, which however would favour also the use of the other techniques. Otherwise LS does not require any particular property except that the particles to be detectable must have an average refractive index different from that of water, which however nearly almost is the case.

The aim of this Master in Science project was to construct core-shell particles that could be suitable for both NMR and LS experiments in coming studies of hydrogels. The goal was to achieve small particles in the range of 100 nm to 1 μm in diameter based on fluorinated oil as the core and a water insoluble polymer as the shell. Also, to avoid complicating interactions with the hydrogel material, it was intended to try to prepare particles with minor amounts or no stabilizer needed for the particle system. The solvent evaporation technique was used as the microencapsulation process, and both dynamic and static light scattering and also NMR diffusometry were carried out to characterize the particles. To study the adsorption behavior of the emulsifier on the surface of the shell polymer, the technique QCM-D (quartz crystal microbalance with dissipation monitoring) was used.

2 THEORY

2.1 Micro- and Nanoencapsulation

A microcapsule is a core-shell system, where the core can be, e.g. an active substance, often dissolved in a liquid and the shell is a polymer. A large number of liquid and solid materials can be encapsulated. Microcapsules are able to immobilize and protect the core substance or the active from UV, moisture, oxygen, etc. Microencapsulation prevents probable chemical reactions between the core and the surrounding environment. Having control over the release of the active material in the core is also another advantage of microencapsulation.[1] Sometimes the term "nanocapsules" is used to emphasize that such microcapsules are in the size range of 10 – 1000 nm.[6]

Besides the methods that have been already mentioned for the preparation of microcapsules, there are some other methods that are used specifically for the preparation of nanocapsules: emulsion-diffusion, nanoprecipitation, double emulsification, emulsion-coacervation, polymer-coating, layer-by-layer, but also solvent-evaporation. The solvent evaporation is a very ordinary technique because it is easy and it does not need any special processing conditions and can also be used to prepare both micro- and nanocapsules. Microencapsulation based on solvent evaporation basically consists of three steps:[4]

(1) preparation of a mixture of an organic phase (composed by polymer, a high vapour pressure good solvent and a non-solvent), and an aqueous phase (composed by water and a proper emulsifier);

(2) emulsification of the organic phase in the aqueous phase;

(3) evaporation of the organic good solvent by continuous mixing or using evaporator.

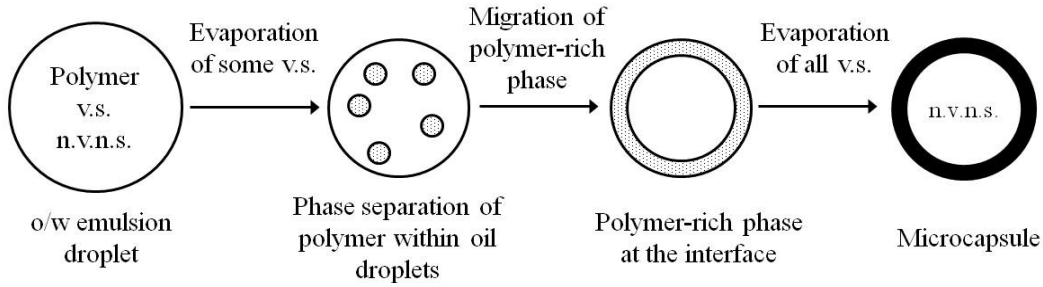

Figure 1: Schematic of the steps of microencapsulation based on solvent evaporation; n.v.n.s., non-volatile non-solvent; v.s., volatile solvent.

Among these three steps, the emulsification of the polymeric solution (organic phase) in the aqueous continuous phase is crucial. The o/w emulsion formation occurs by agitation of two immiscible liquids. Normal stirrer (impeller), homogenizer, or microfluidizer are suitable instruments for dispersing the oil phase in the continuous aqueous phase. Depending on the desired size and size distribution any of these techniques can be used. The one which is able to induce stronger shear forces and more turbulence will give smaller droplet sizes and more narrow size distributions.

An impeller is a rotating blade which is connected to a shaft. It imposes bulk motion (shear stress) and is used to mix immiscible and highly viscous liquids. A homogenizer is based on a rotor/stator principle (see Figure 2) and is used for dispersing and homogenizing immiscible liquids and solid particles. Both these techniques are thus based on applying a shear stress to produce a turbulent flow, while the microfluidizer is based on a special technology, in which the flow is laminar and the droplets are formed at the site of addition of oil phase to the continuous phase.[7] Droplet size and size distribution is controlled in a microfluidizer by varying the processing pressure and the number of passes through the instrument.

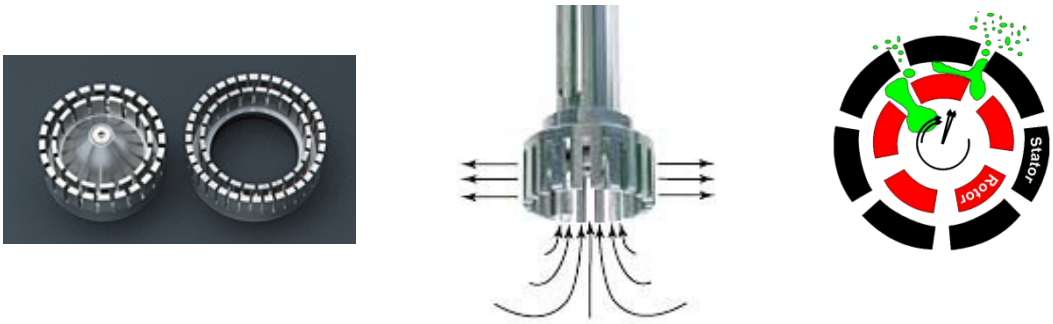

Figure 2: Schematic rotor/stator and its function.[8]

Since the size of the capsules or particles formed is related to the size of the droplets in the primary emulsion, all the parameters that influence the droplet size in the emulsion will affect the particle size in the final suspension as well. Besides processing parameters that already have been mentioned, there are many other important parameters that influence the size and size distribution of the particles during emulsification, such as nature and concentration of emulsifier, polymer concentration, oil viscosity, presence of a co-solvent (e. g. acetone), polymer/oil ratio,[9] temperature, and time of emulsification.[4,10] Most of these parameters influence either the viscosity of the oil phase or the aqueous phase. For instance, polymer concentration, type and amount of solvent, temperature, and oil viscosity have great influence on the viscosity of the oil phase, while type and concentration of emulsifier affect the aqueous phase viscosity.

On the other hand, droplet disruption as a result of applied shear depends on the viscosity of both the dispersed and continuous phases. The lower the viscosity of the dispersed phase (oil phase), the less energy is needed to disrupt the droplets and droplet break-up is easier. The higher the viscosity of the continuous phase, the stronger the viscous forces that generate stress at the drop surface, which facilitates the droplet disruption. However, with a polymer as emulsifier in the continuous phase the result can be different; the polymer may restrain the turbulence, which will result in a less efficient droplet disruption. Thus, with polymers as emulsifiers, the droplet size first decreases with increasing concentration, but can then start to increase after a certain concentration when the effect of the restrained turbulence becomes important. On the other hand, also the viscosity ratio of both phases ($\eta_{oil}/\eta_{aqueous)}$ has an effect on the droplet break-up; an increase in this ratio will result in an increase in droplet size.[11] Accordingly, the factors that influence the viscosity will directly influence the size and size distribution of the finally formed particles.

Moreover, there are parameters during the evaporation process that might influence the size of the particles such as speed and temperature of evaporation, as well as emulsifier concentration.[12] The important thing during evaporation is to prevent coalescence and to get complete solvent removal, in order to get particles of the similar size and size distribution as the droplets in the emulsion.[12]

Although the solvent evaporation method is an easy-to-use method and has been used for preparation of both micro- and nanocapsules, some research[5] has demonstrated that the presence of high molecular weight species e.g. polymers in the interface of the oil and the aqueous phases, can limit the diffusion of the solvent through the aqueous phase. The evaporation and capsule formation are then difficult to control in the case of nanoencapsulation. Also, other research[13] showed that nanocapsules might not be processed successfully with the direct solvent evaporation technique because of the mechanical stress induced from the bubbles in the aqueous phase. Therefore, solvent evaporation is perhaps not the best method to make nanocapsules. Nevertheless, the convenience of this technique would be a reason to pursue trying to optimize parameters for the solvent evaporation method to prepare nanocapsules, as was one aim this thesis.

2.2 Phase Diagram

In order to prepare a suitable oil phase to make core-shell particles, the selection of right solvents and proper concentrations and having knowledge about the thermodynamics of mixing and kinetics of phase separation in, e.g., a ternary system, are important issues. A phase diagram summarizes the phase behaviour of a mixture at equilibrium and shows at which concentrations all the components are completely dissolved in each other and at which concentration of each component phase separation will start. Binary and ternary phase diagrams can be constructed both theoretically and experimentally. Knowledge about the kinetics can only be obtained in detail by experiments, but some guidance might be obtained from considering principles of diffusion.

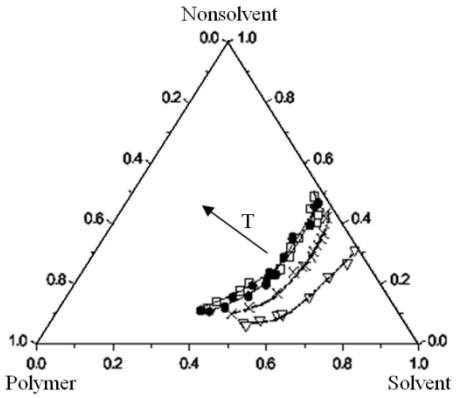

Figure 3: Typical ternary phase diagram for the polymer/solvent/nonsolvent system

A ternary phase diagram for nonsolvent/solvent/polymer system can be made theoretically based on Flory-Huggins theory[14] for three components. (A typical ternary phase diagram is shown in Figure 3) Although the Flory-Huggins theory first was developed for thermodynamic behaviour of binary systems it was later extended

to three component systems by Tompa[15]. According to Tompa's theory the Gibbs free energy of mixing for a ternary system is given by:[16]

$$\Delta G = RT\left[n_1 \ln \phi_1 + n_2 \ln \phi_2 + n_3 \ln \phi_3 + g_{12}(u_2) n_1 \phi_2 + g_{23}(v_3) n_2 \phi_3 + \chi_{13} n_1 \phi_3\right] \qquad \text{Eq. 1}$$

The subscripts refer to nonsolvent (1), solvent (2), and polymer (3). n_i and ϕ_i are the number of moles and the volume fraction of component *i*, respectively. *R* is the gas constant, and *T* represents the absolute temperature. χ_{13} is the concentration-independent nonsolvent/polymer interaction parameter, while g_{12} and g_{23} are the concentration–dependent nonsolvent/solvent and solvent/polymer interaction parameters. u_2 is the volume fraction of solvent on a polymer free basis, and v_3 is the volume fraction of polymer on the a nonsolvent free basis, i.e. $u_2 = \phi_2/(\phi_1+\phi_2)$ and $v_3 = \phi_3/(\phi_2+\phi_3)$.

In order to obtain a phase diagram from Eq. 1, the interaction parameters should be known which can be achieved experimentally. In this work, complete phase diagrams were not made for the present components. However, phase diagrams with quite the same components have been presented by other researchers,[12,17] and therefore used as guidance in this work. The concentrations of the components were chosen so that the systems corresponded to the one phase regions.

2.3 Diffusion

Translation motions in solution are diffusion and fluid flow. The translational motions of a species not only reflect intrinsic properties of the species itself (such as size, etc.) but can also shed light on the surrounding environment (such as material microstructure and dynamics). Self diffusion is the random thermal motion of molecules or small particles in a liquid at thermal equilibrium. It is possible to imagine it as Brownian motion where a small suspended particle is constantly and randomly hit by collisions with molecules of the liquid and makes particle jumps (see Figure 4). Translational diffusion is characterized by a diffusion coefficient which can be calculated from the Stokes-Einstein equation[18] (for the simple case of a spherical particle at infinite dilution):

$$D = \frac{k_B T}{6\pi\eta R_h} \qquad \text{Eq. 2}$$

where k_B is Boltzmann constant (J/K), *T* is temperature (K), η is the viscosity of the liquid (Pa s), and R_h is the hydrodynamic radius of the particle (m), which gives D in m^2/s.

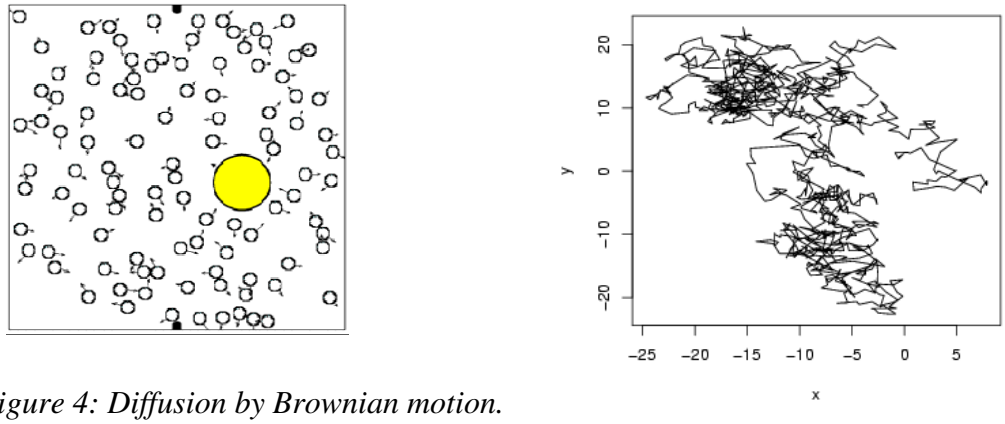

Figure 4: Diffusion by Brownian motion.

According to the Stokes-Einstein equation the diffusion coefficient of a suspended particle (except for the universal constant and absolute temperature) depends on the viscosity of the liquid and on the size of the suspended particles.

On the other hand, based on Fick's first and second laws, the diffusion coefficient can be calculated from the mean-square-displacement, MSD, which states that for free diffusion the MSD changes linearly with time:

$$\left\langle \Delta r^2(t) \right\rangle = 2\,n\,D\,t \qquad \text{Eq. 3}$$

where D is the diffusion coefficient (m^2/s), $<\Delta r^2(t)>$ is the MSD (m), n is dimension, and t is time (seconds). According to this definition the diffusion coefficient depends on how the mean-square-displacement changes with time. For free diffusion, the diffusion coefficient calculated from this equation is constant while it is a function of time for restricted diffusion. Measuring the mean-square-displacement with any technique e.g. NMR and dynamic light scattering gives the possibility to calculate the (average) hydrodynamic radius of the diffusing species at zero concentration (free diffusion) from Eqs. 2 and 3 as

$$\frac{\left\langle \Delta r^2(t) \right\rangle}{2n \cdot t} = \frac{k_B T}{6\pi\eta R_h} \qquad \text{Eq. 4}$$

Thus, the size of diffusing species is one of the intrinsic properties that can be determined by measuring the diffusion coefficient.

Moreover, different diffusion regimes exist and are classified depending on the behaviour of the diffusing species and how they are influenced by the environment.[19] These regimes can be described by an MSD proportional to t^{α}. If $0 < \alpha < 1$ the regime is called subdiffusion for which the MSD increases slower than is the case for free diffusion. Such behaviour can be expected when the particles are restricted to move in, e.g. a hydrogel system, where obstruction can occur due to a microheterogeneous structure. Moreover, the increase in $\left\langle \Delta r^2(t) \right\rangle$ is no longer linear. However, when $\alpha > 1$ the MSD increases again in a non-linear manner but faster than for free diffusion and the distribution of jump distances is wide. The diffusion regime is called

superdiffusion or Levy flight and is typical for a particle in, e.g. a turbulent flow like smoke from a chimney; see Figure 5.

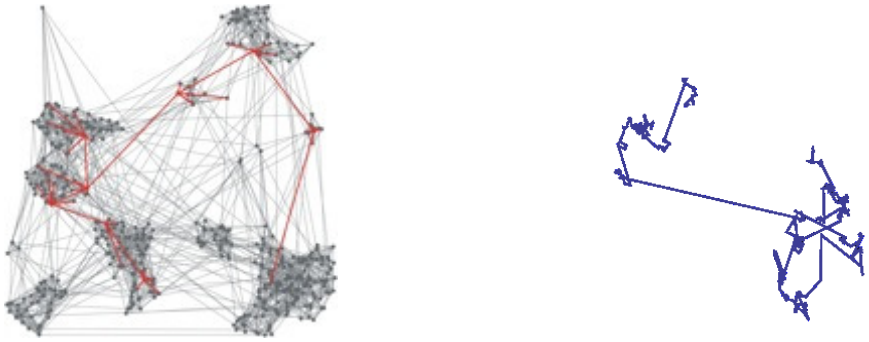

Figure 5: Schematic illustration of superdiffusion or Levy flight showing the Brownian motion of a particle that occurs in a separate region followed by a jump to another Brownian region.

2.4 Principle of Light Scattering

Light scattering is a frequently used technique to investigate, e.g., polymers in solution, and colloidal particles. The theory of light scattering was first developed by Lord Rayleigh for small particles (compared to the wavelength of the incident light) and was extended by Debye for large particles and by Mie for all particles without any particle size limitation.[20]

The Rayleigh theory states that the origin of scattered light is a complex interaction between the incident light and the molecular structure of the scattering object. When incident light interacts with a particle, the electron orbit of the molecules of the particle is periodically perturbed with the same frequency as the electron field of the incident light. The oscillation of the electron cloud causes an induced dipole moment within the molecule. The oscillating induced dipole moment is manifested as scattered light. The scattering process is called elastic when the scattered light frequency is the same as the incident radiation frequency (Rayleigh scattering). Since molecules in solution are in a random motion there will be scattered light of several frequencies around the frequency of the incident radiation. Therefore, light scattering is sometimes called "quasi-elastic-light-scattering". In this molecular theory the fundamental parameters are the polarizability and the medium refractive index. Besides this molecular theory there is a thermodynamic theory which describes the origin of the scattered light with another approach. In the Einstein-Smoluchowski thermodynamic approach, the interaction of the radiation field with the inhomogeneities, caused by the random motions of the molecules, is a result of localized microscopic fluctuations of density and thus the dielectrical constant is considered. This thermodynamic theory explains why a pure liquid can scatter light as the result of density fluctuations. Both Rayleigh (and the further developed Rayleigh-Gans-Debye) and Einstein-Smoluchowski theories are applicable for particles when

the relation between size, wavelength of light and refractive indices obeys Eq. 5 below: For larger particles the Mie theory was developed.

$$R < \frac{\lambda_o}{2\pi\left|n_m - n_p\right|}; \quad \left|n_m - n_p\right| < 1 \qquad \text{Eq. 5}$$

where R is the radius of the particles, λ_o is the wavelength of the light, and n_m and n_p are the refractive indices of the medium and the particles, respectively

The physical concept of the Mie theory is the same as the Rayleigh theory, so that the oscillation induced polarization within the particle is due to the incident light field, and light scattering from the particle is the result of those oscillations. However, in the Mie theory a particle is considered to have contributions of a series of electrical and magnetic multipoles located in the particle, instead of assigning one single dipole to the particle (as in the Rayleigh theory). For large particles relative to the light wavelength, the Mie theory predicts the direction of the scattered light to occur at different angels.

Light scattering instruments for both static and dynamic light scattering techniques (SLS and DLS respectively) are equipped with laser light which is a coherent and monochromic source of light. A schematic instrument set up for SLS and DLS is shown in Figure 6.

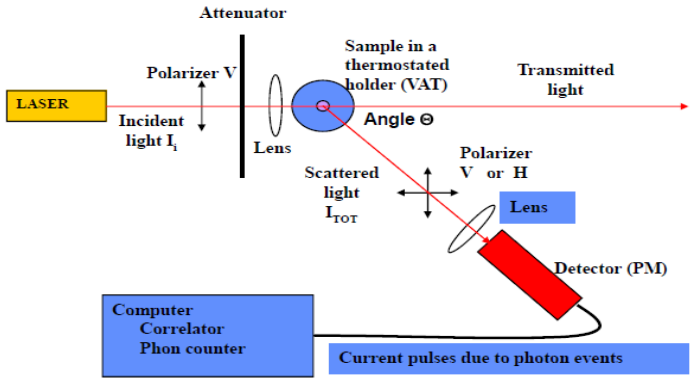

Figure 6: Instrument set up for SLS and DLS

2.4.1 Static Light Scattering

Static light scattering is a technique that has been used mostly to characterize the physical chemical properties of species in solution, such as polymers in solution, colloidal suspensions, and micellar systems. In a light scattering instrument, scattered light is detected at different angles. The instrument measures the total intensity of the light as a function of angle and/or concentration. The quantity of interest of the scattered light is the so-called Rayleigh ratio, R_Θ, which can be calculated from the measured intensities of solvent and solution:

$$R_\theta = k\frac{I_{solution} - I_{solvent}}{I_{incident}} \qquad \text{Eq. 6}$$

where I is the intensity of the indicated system, and $k/I_{incident}$ arises from calibration. The Rayleigh ratio depends on the angle of observation (see Figure 5) through the scattered wave vector, q, which is defined as:

$$q = \frac{4\pi n_0}{\lambda_0} sin\left(\frac{\theta}{2}\right) \qquad \text{Eq. 7}$$

where n_0 is the refractive index of the solvent, λ_0 is the incident light wavelength in vacuum, and θ is the angle of observation.

On the other hand, the Rayleigh equation below describes the relation between the intensity of the scattered light (Rayleigh ratio) and physical chemical properties of the particle in solution accordingly, which is the simplified form by Zimm and which is fulfilled at low concentrations:

$$\frac{Kc}{R_\theta(c,q)} = \frac{1}{M_w P(\theta)} + 2A_2 c + 3A_3 c^2 + ... \qquad \text{Eq. 8}$$

where M_w is the average molecular weight of the species, $P(\theta)$ is the form factor (particle scattering factor), c is the particle concentration, A_2 is the second virial coefficient (a measure of how good the solvent is), and K is an optical constant which is defined as:

$$K = \frac{4\pi^2 n_0^2}{\lambda_0^4 N_A}\left(\frac{dn}{dc}\right)^2 \qquad \text{Eq. 9}$$

where dn/dc is the changes in refractive index of the solution as a function of the changes in concentration, and N_A is Avogadro's constant. The Zimm equation can be used in order to analyse the data from static light scattering in different ways; one way is to plot $Kc/R_\theta(c,q)$ vs q^2+kc for different concentrations and different angles. The factor k in this plot is used to expand the x-axis in a suitable way and can be chosen arbitrary to give a foreseeable plot. This kind of plot was proposed by Zimm in 1948,[20] and is called the Zimm-plot. The Zimm-plot is used frequently to analyse static light scattering data to determine M_w, R_g, and A_2.

The form factor or particle scattering factor, $P(\theta)$, is the angular dependence of the scattered light intensity. The angular dependence arises from the light scattered from different positions in the same particle and this happens when the particle is big enough compared to the wavelength of the incident light. In fact, it shows how the intensity will change with the size and shape of the particle. The form factor has been theoretically calculated for several different types of systems and are available in several papers.[21] For example, the form factors for the hard sphere and the core-shell particle are given below, respectively:[22]

$$P(\theta)=\left[\frac{3}{(rq)^3}\left(sin(rq)-rq\,cos(rq)\right)\right]^2 \qquad \text{Eq. 10}$$

$$P(\theta)=\left[\frac{\left(m_1^2-1\right)\left(m_2^2+2\right)V_1R(r_{in}q)+\left(m_2^2-1\right)\left(m_1^2+2\right)\left(V_TR(r_{total}q)-V_1R(r_{in}q)\right)}{\left(m_1^2-1\right)\left(m_2^2+2\right)V_1+\left(m_2^2-1\right)\left(m_1^2+2\right)V_2}\right] \qquad \text{Eq. 11}$$

where r is the radius of the hard sphere, q is the scattering wave vector in Eq. 6, $m_1=n_1/n_0$, n_1 is the refractive index of the core, and n_0 is the refractive index of the medium, $m_2=n_2/n_0$, n_2 is the refractive index of the shell, V_1 is the volume of the core, V_2 is the volume of the shell, V_T volume of the total particle, and finally $R(rq)$ is defined in Eq. 12:

$$R(rq)=\frac{3(\sin rq-rq\cos rq)}{(rq)^3} \qquad \text{Eq. 12}$$

By plotting $P(\theta)$ vs. q, e.g. for hard spheres, see Figure 7(a), it is possible to estimate the size of the particle. It is seen that when the particles are very small, the angular dependence in $P(\theta)$ is lost. For larger particles a pronounced θ-dependence can be seen, even with minima for very large particles. In the plot of log $P(\theta)$ vs. qr (see Figure 7(b) the first minimum for large particles is (generally) located at $qr = 4.49$, where r is the radius of the particle. Thus, finding the first minimum in $P(\theta)$ vs q gives the radius from $r = 4.49/q_{min}$ provided the particle is big enough to give a minimum.

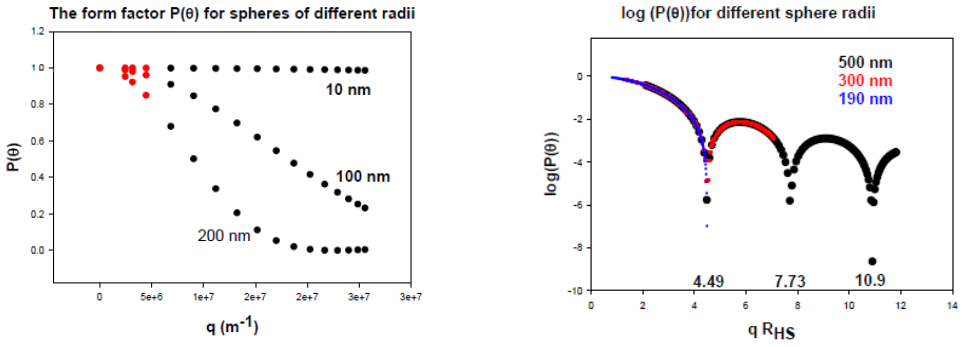

(a) (b)

Figure 7: (a) plot of P(θ) vs. q for hard spheres of different radii, and (b) log P(θ)vs. qr for spheres of different radii. R_{HS} is the hard sphere radius.

The Guinier approximation is also a very useful approach to evaluate static light scattering data to determine R_g.[20,23] It states that when

$qR_g \to 0$, then $P(\theta) = 1 - q^2 R_g^2/3$ for any type of system at zero or very low concentrations.

Thus, by plotting $ln\left(\frac{R_\theta}{Kc}\right)$ vs. q^2 for data at zero concentration, which is called a Guinier plot, it is possible to determine R_g from the slope of the plot and M_w from the intercept, provided the plot is linear (see Eq. 8). Often this means that only data at low q-values can be used, if at all. The Guinier plot and plot of $P(\theta)$ vs. q were used in this work to estimate R_g and the type of particle using a Sigma plot program (SigmaPlot 2000, SPSS Inc.). It is seen that taking the logarithm of the reciprocal of Eq. 8, and subtracting $ln(M)$, where M is an apparent molecular weight, the resulting experimental data for low concentrations should be forced to pass $ln(P(\theta=0))=0$ according to the Guinier approximation. The experimental data can then be compared with different theoretical plots of $P(\theta)$, provided the experiments are carried out at low concentrations as in the present work.

2.4.2 Dynamic Light Scattering

Dynamic light scattering is a technique to determine, e.g., sizes and size distributions of small particles in suspension or polymers in solution. Moreover, it can be used to study the structural behaviour of concentrated polymer solutions or gel systems. As mentioned before monochromatic and coherent light similar to SLS laser light is needed. In DLS the time dependent fluctuations in the intensity of the scattered light are recorded with a fast computer, the so-called correlator. These fluctuations arise from the particles movement in the observation volume due to Brownian motion of particles. The relation between these fluctuations during an experiment is calculated based on a mathematical operation called autocorrelation and results in the time correlation function (Eq. 13) in the correlator:

$$G^2(t) = \langle I(0) I(t) \rangle \qquad \text{Eq. 13}$$

where $I(t)$ is the intensity at time t.

The $G^2(t)$ can be called a memory function and it contains the measured raw data. The $G^2(t)$ is normalized through a symmetric normalization proposed by ALV:[23]

$$G^2(t) \xrightarrow{normalization} g^2(t)$$

where $g^2(t)$ is the normalized intensity correlation curve. This correlation curve is normally displayed as $log\ (g^2(t)-1)$ vs. $log\ t$ in order to have the possibility to follow the curve for a long time and to have good control over the background (see Figure 8).

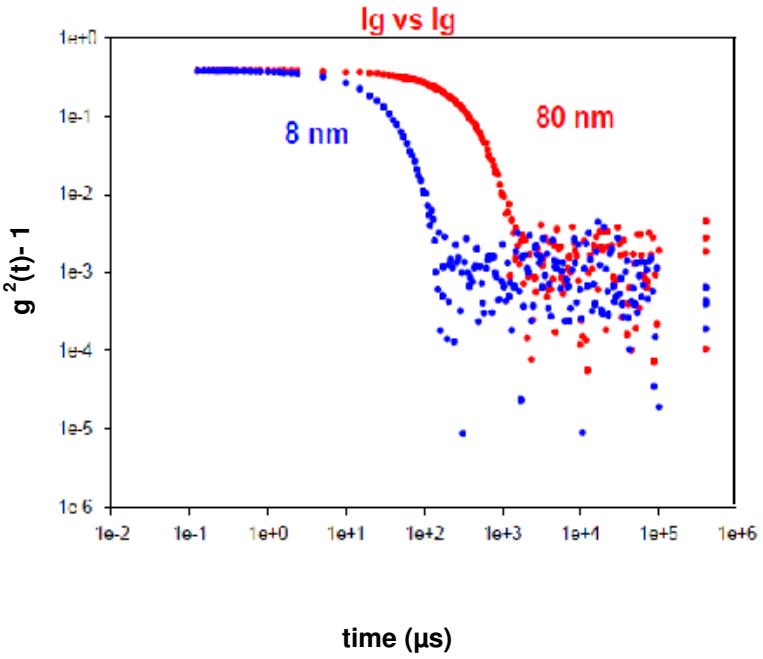

Figure 8: Correlation curves for two kind of spheres; the blue curve is for spheres with R_h=8nm, and the red curve is for spheres with R_h=80nm

The normalized intensity correlation function $g^2(t)$ is related to the normalised field correlation function called $g^1(t)$, which contains the information of interest through the Siegert relation:

$$g^2(t) = 1 + \beta \left| g^1(t) \right|^2 \qquad \text{Eq. 14}$$

where β is a correction factor that depends on the detection aperture and counting rate; in fact it is an instrument constant. It takes a value between 0 to (ideally) 1 depending on the construction of the instrument, and for the instrument that has been used in this work β=*0.37*. However Eq. 14 is only valid for ergodic systems, i.e. for systems where the time average of a property is independent of where in the system the property is studied. This is expressed as the time average being equal to the ensamble average. A particle dispersion at low concentrations is one example of an ergodic system, while a gel normally is non-ergodic (contains heterogeneous parts).

The field correlation function $g^1(t)$ contains dynamic information of the system studied. Different theoretical descriptions exist for $g^1(t)$, the simplest one describing the field correlation function for monodisperse, non-interacting particles as follows:

$$g^1(t) = \exp(-\Gamma t) = \exp\left(-\frac{t}{\tau}\right) = \exp\left(-q^2 D t\right) \qquad \text{Eq. 15}$$

where Γ is the relaxation decay rate (sec^{-1}), τ is the relaxation time (sec), D is the diffusion coefficient (m^2sec^{-1}) defined in Eq. 2, and q is the magnitude of the scattering wave vector (m^{-1}) as defined in Eq. 7. In the case of polydisperse systems $g^1(t)$ will decay as a sum of exponentials.

In general, the field correlation function can be described by:

$$g^1(t) = \exp\left(-\frac{\langle \Delta r^2(t) \rangle}{6} q^2\right) \qquad \text{Eq. 16}$$

where $\langle \Delta r^2(t) \rangle$ is the MSD for the scattering species, and which can be written, e.g. as in Eq. 3. Equation 16 is the starting point for analysis of, e.g., microrheology experiments.

In order to analyse the data from DLS, several algorithms exist and which are based on cumulants, the Contin procedure, and/or on some non-linear models like the Schultz model.[23] The Contin algorithm is the most frequently used algorithm which preferentially is used to get the distribution of relaxation times, the standard deviation (σ) and the coefficient of variation (CV = the relative standard deviation) of the distribution, from which a distribution of, e.g. sizes can be obtained. However precautions should be taken when the Contin algorithm is used. Thus, for very narrow distributions with a width of CV < 0.07, the Contin algorithm sometimes does not give the correct distribution but the cumulants algorithm might work fine. When the distribution is not too narrow and CV > 0.07, the Contin model will lead to a reasonable distribution. However, sometimes when the CV is very small, the ALV cumulants analysis has been found to report a negative value of one estimated parameter μ_2 related to the polydispersity index (PDI) by PDI=μ_2/Γ^2 (=CV^2) where Γ is the average relaxation rate of the system. A negative PDI is of course not physically possible, and for some data the non-linear Schultz model is then better to use.

2.5 Nuclear Magnetic Resonance Diffusometry (NMRd)

NMRd is a very powerful technique to measure the self-diffusion of species in a wide range of sizes (from small water molecule to a few micrometer particles) in variety of mediums. The diffusion coefficient obtained from NMRd can be used to determine, e.g, the hydrodynamic radius of the species, membrane permeability, and effects of chemical exchange. In NMRd two gradient pulses are used, of which the first gradient encodes the position of the nuclear spin. In fact, the first gradient is labelling the spin magnetically and gives the possibility to follow the translational motions during an observation time, Δ. The labelling is decoded after the observation time by applying the second gradient pulse. The use of pulse field gradients in Spin-Echo Pulsed Field Gradient experiments was suggested by Stejskal and Tanner,[24] and the experimental layout is schematically shown in Figure 9.

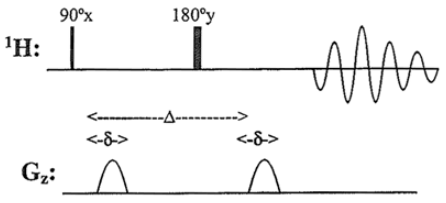

Figure 9: The Stejskal-Tanner spin-echo pulsed field gradient experiment.

The gradient pulses are often sine-shaped. The normalised signal attenuation depends on the strength, g, and length, δ, of the gradient pulses, the time between two gradients (observation time), Δ, and the diffusion coefficient of the species. The normalised signal intensity for the square shaped gradient is then as described by Stejskal-Tanner in Eq. 17:

$$I/I_0 \propto \exp\left(\gamma^2\delta^2 g^2\left(\frac{\Delta-\delta}{3}\right)D\right) \qquad \text{Eq. 17}$$

where I and I_0 are the NMR signal intensities with and without gradients and γ is the gyromagnetic ratio constant. The Stejskal-Tanner equation can be written as:

$$I/I_0 = \exp(-kD) \qquad \text{Eq. 18}$$

where $k = \gamma^2 g^2 \delta^2\left(\frac{\Delta-\delta}{3}\right)$. Therefore it is possible to determine the diffusion coefficient, D, from a nonlinear least square fit of log(I/I_0) vs k with the slope of D. Then using the Stokes-Einstein equation (Eq. 2) it is possible to calculate the hydrodynamic radius of the (spherical) species.

2.6 Quartz Crystal Microbalance with Dissipation Monitoring (QCM-D)

The QCM with the dissipation monitoring technique is used for measuring macromolecule adsorption and structural properties of them on a surface in a liquid. Basically QCM-D is based on the piezoelectric properties of quartz. A thin quartz disc placed between two electrodes (typically gold electrodes), is subjected to an AC voltage across the electrodes. The piezoelectric material i.e. the quartz crystal, starts to oscillate at a specific (resonance) frequency which is related to the mass of the crystal. Adsorption of any spices on the surface of the crystal results in an increase in the total mass and consequently a change in the oscillation frequency. When the adsorbed layer is a thin rigid film, the amount of the absorbed layer can be calculated using Sauerbrey equation:[25]

$$\Delta m = \frac{\Delta f\, C}{n} = \rho_f\, \delta_f \qquad \text{Eq. 19}$$

where C is the mass sensitivity constant (= 17.7 ng/cm^2), n is the overtone number, ρ_f is the effective density of the adhering layer (ng/cm^3), and δ_f is the estimated thickness (cm). However for non-rigid or flexible adsorbed layers (films) which are quite common in a liquid phase, the Sauerbrey equation is invalid. In fact, the Sauerbrey equation underestimates the mass at the surface, since a soft film will not fully follow the crystal's oscillation. A viscoelastic (soft) film dissipates some parts of

the crystal's oscillation; this dissipation (D) shows the viscoelasticity of the film according to:[26]

$$D = \frac{E_{lost}}{2\pi E_{stored}} \qquad \text{Eq. 20}$$

where E_{lost} is dissipated energy (J) and E_{stored} is stored energy (J). The dissipation of the crystal is measured by recording the response of a freely oscillating crystal vibrating at its resonance frequency. By measuring frequencies and dissipation at different overtones and applying viscoelastic models a soft film can be characterized. Either the Voigt model is used, which is a model for a viscoelastic solid[27] or the Maxwell model which is for a viscoelastic liquid.

In this work the measured dissipations and frequencies were modelled using the Voigt model given by Eq. 21 below:[27]

$$\sigma(t) = E\varepsilon(t) + \eta\frac{d\varepsilon(t)}{dt} \qquad \text{Eq. 21}$$

where σ is stress (it can be shear stress or normal stress,(Pa)), ε is strain (unitless), η is viscosity (Pa s), and E is the modulus of elasticity (Pa).

2.7 Scanning Electron Microscopy

In a scanning electron microscope, SEM, an electron beam is used to scan the surface of the sample. To get information from the scan, both primary electrons (the electrons from the beam that are backscattered) and secondary electrons (the electrons that are emitted from the sample) are detected. Photons that are emitted from the sample are also detected. The scattering patterns give information about topography, morphology and composition. Topography describes what the surface looks like, morphology gives the shape and size making up the sample, while the composition shows the different elements in the sample and the relative amounts of them. SEM has a focus that are called the Depth of Field, which means that it has a large depth of focus, which makes it possible to produce an image that appears 3-dimensional.

Specimen preparations are needed before using SEM. The sample needs to be in vacuum and therefore the sample can not contain any liquids that will vaporize under that condition. The samples need to be conductive in order to be examined. Non-conductive samples have to be coated with an electrically conductive film. If the sample need to be in a wet environment, or if the sample is non-conductive, an instrument called Environmental SEM, ESEM, can be used.

3 EXPERIMENTAL

3.1 Materials

3.1.1 Shell Polymers

PMMA (poly (methyl methacrylate)) is an amorphous synthetic polymer made of methyl methacrylate monomers (repeating unites), (see Figure 10). Commercially, it can be found under the name of Plexiglas, Perspex, Acrylex, and also other names. It is produced by emulsion polymerization, solution polymerization, and also bulk polymerization. PMMA has a glass transition temperature (T_g) around 105°C and it can be varied for different molecular weight. It is insoluble in water and soluble in organic solvents, and it has good mechanical properties. Three PMMA with different molecular weight 350 kD, 120 kD, and 95 kD, bought from Sigma-Aldrich, were used in this Thesis work.

Poly(methyl methacrylate-co-methacrylic acid) is also an amorphous synthetic copolymer made of both methy methacrylate (MMA) and methacrylic acid (MA) repeating unit and with a ratio of MMA to MA that can be varied; see Figure 9. The one used in this work was bought from Sigma-Aldrich with a molecular weight of 34 kD and with MMA to MA ratio equal to 1:0.016 and a T_g = 105°C

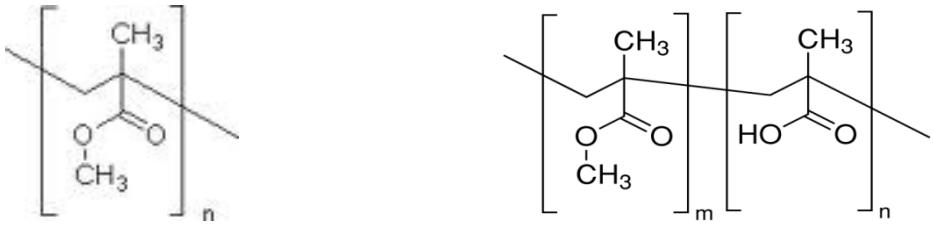

(a) (b)

Figure 10: Chemical structures of (a) poly (methyl methacrylate) and (b) poly (methyl methacrylate-co-methacrylic acid).

3.1.2 Core Oils

When the core shall contain an oil (as intended here) it should have some very important properties. First, it should have water solubility as small as possible for reasons discussed earlier. Second, the solubility in the solvent used for the polymer shell material should meet the requirements of how much of the oil that should be present in the final core-shell particles. Third, a very high interfacial tension between the core oil and aqueous phase is needed. Fourth, the core oil should have a very high boiling point and very low vapour pressure not to be removed during solvent evaporation. Finally, specifically for this Thesis project, the oil should be detected by NMR. Thus, it should contain atoms such as F, H, or C^{13}. Also, to be detectable by light scattering its refractive index should be different from the polymeric shell and the medium (water). Besides, it is preferable that the solubility of the core oil in the polymeric shell is as small as possible. Considering all the requirements above fluorinated oils were chosen for the present work.

Fluorinated oils or perfluorocarbons are composed of carbon and fluorine bonded together. They have very low viscosity compared to the molecules with the same molecular weight due to their weak intermolecular interaction. They have very low surface tension and very low vapour pressure, also their refractive index is notable. Further, they have restrictive miscibility or solubility in organic solvents, but very low solubility in water. Fluorinated oils are biologically inert and chemically stable due to the strength and nature of carbon-fluorine bonds. Thus, they hardly interact with other materials. Three different fluorinated oils were used in the work, bought from Sigma-Aldrich. Perfluorodecalin is an odourless, colourless fully-fluorinated liquid with density=1.917 g/cm^3, vapour pressure = 0.83 kPa, boiling point = 142°C, and refractive index = 1.313. It has limited miscibility in chloroform and dichloromethane (which were used as solvents for the polymer shell material). Perfluorooctane has nearly the same properties as the previous one with density = 1.76 g/cm^3, vapour pressure < 1.3 kPa, boiling point=104°C, and refractive index = 1.28, but it is partially miscible in chloroform.

Perfluorodecalin (a)

Perfluorooctane (b)

Figure 11: Chemical structure of (a) perfluorodecalin and (b) perfluorooctane

In order to compare fluorinated core particles with other kind of particles, dodecane was also used as the core oil. Dodecane (Sigma-Aldrich) is an alkane hydrocarbon with chemical formula $C_{12}H_{26}$, density = 0.75 g/cm^3, vapour pressure = 0.2 kPa, boiling point = 216.2°C, and refractive index = 1.42. It is miscible in chloroform and dichloromethane and rarely soluble in water.

Moreover, to use the oil absorption technique[28] for encapsulation, (see section 3.2 below) one other fluorinated molecule, trimethyl(pentafluoro phenyl)silane (Sigma-Aldrich), was used. It is a clear, colourless liquid with density = 1.261 g/cm^3, boiling point = 170°C, and refractive index = 1.433. Vapour pressure for this molecule was not available.

Figure 12: Chemical structure of trimethyl(pentafluoro phenyl)silane.

3.1.3 Solvent

In the solvent evaporation method the solvent selection plays a very crucial role in the evaporation stage. Therefore, some requirements should be met by the solvent when used for preparing microparticles with this method. Immiscibility of the solvent with water is the first requirement, but solvent diffusion into the aqueous phase is indeed needed to get a control of the rate of evaporation. The diffusion of the solvent depends on its water solubility; very low water soluble solvents would diffuse very slowly into the aqueous phase and evaporate slower, while in fact a highly water immiscible solvent retards evaporation rate,[5] (as also found in the present experiments). Second, the complete dissolution of both oil and polymer in the organic solvent is very important. The possibilities for this are best determined by a phase diagram. Furthermore, the lowest heat of evaporation or the highest vapour pressure is required to enhance and speed up the removal of the solvent from the water/air interface by evaporation.[29]

The solvents used in this work were dichloromethane (DCM; Sigma-Aldrich)), which is miscible with organic solvents, has a very low miscibility with water (13g/l at 20°C), a boiling point = 40°C, and vapour pressure = 47 kPa at 20°C, and chloroform, an effective solvent for alkaloids, with very low solubility in water (8g/l at 20°C), a boiling point = 61.2°C, and vapour pressure = 21.2 kPa at 20°C.

3.1.4 Emulsifier

As mentioned before, the emulsifier has a crucial role both during the emulsification and evaporation stages. In this work two different emulsifiers were used; polyvinyl alcohol (PVA, Sigma-Aldrich)) with M_w=88 kD and 88% hydrolyzed, poly(methacrylic acid) (PMAA, Polyscience Inc.) with M_w=100 kD.

Figure 13: Chemical structure of polyvinyl alcohol and poly(methacrylic acid).

3.1.5 Other Materials

Acetone (Sigma-Aldrich) was used in most of the formulations to reduce the viscosity of the oil phase and also to facilitate the evaporation. Ethanol (99.5 v%, Kemetyl AB, Sweden) was used to clean the cyvettes for light scattering (Hellma GmbH&Co, Germany, LS circular LS cyvettes). The water was highly purified through a Milli-Q Academic System equipment and used as it was for preparing the aqueous solution, but it had been filtrated with 100 nm filters (Minisart, non-pyrogenic) and degassed for the light scattering samples. Helmanex II (Hellma) was used for cleaning the cuvettes, while ordinary glass vials were used for DLS sample preparations. Hollow sphere particles (30% w/w, average particle size 380 nm, Rohm & Haas, Germany) and polystyrene latex particles (CML latex, 4%w/v, 0.1µm, CV=0.05, Molecular Probes Inc. U.S) were used as references in light scattering measurements.

3.2 Synthesis of Microcapsules

Microcapsules were prepared with the solvent evaporation method using both a high shear homogenizer and a microfluidizer. For both set-ups the oil phase and the aqueous phase were prepared individually. The emulsifier (PVA or PMAA) was dissolved in Milli-Q water at 85-90°C for 2 h and was left overnight to slowly attain room temperature. The concentration of the emulsifier was different for the different formulations, some of which are shown in Table 1. PMMA or co-polymer was dissolved in the organic solvent at room temperature for 1h after which the oil was added. The mixture was continuously stirred to get the complete dissolution of the oil.

The aqueous phase (80 gr) was stirred with a rotor/stator homogenizer (Kinematic) at 5000 rpm, while the organic phase (80 gr) was added during 60 s. The temperature was varied for the different protocols. The stirring was raised to 15000 to 20000 rpm for one hour for different samples. A processed mixture was immediately after one hour poured into 120 gram of aqueous phase placed in a ventilated hood while stirring slowly (400 rpm) with a magnetic stirrer to allow for the evaporation of the dichloromethane (or chloroform) and the acetone. Once a particle dispersion had formed, it was diluted with water for analysis, e.g. size and size distribution.

Table 1: Formulations and processing conditions for different samples prepared by rotor/stator homogenizer. The solvent used for all formulation was chloroform.

Sample code	PVA(%)*	PMAA(%)*	M_W/kD PMMA	M_W/kD Copolymer	Oil	Temp (^oC)	Acetone (%)	Shear (rpm)
BF1	1		350		F.D	20	5	15000H
BF2	1		350		F.D	20	5	20000H
BF3	2		95		F.O	35-45	3	20000H
BF4	1		95		F.O	35-45	10	20000H
BF5	2		95		F.O	35-45	10	20000H
BF6		2	120		F.O	25-30	10	19000H
BF7		1	120		F.O	25-30	10	19000H
BF8	2		120		F.O	35-45	5	20000H
BF9	5		95		F.O	35-45	10	17000H
BF10	2		95		F.O	35-45	10	20000K
BF14	2			34	F.D	25-30	10	19000H
BF15	1			34	F.D	25-30	10	19000H
BF17	2		95		D.D	25-30	10	19000H
BF18		1		34	F.D	25-30	10	19000H
BF19		2		34	F.D	25-30	10	19000H

*F.D=perfluorodecalin; F.O=perfluorooctane; H=Heidolph; K=Kinematic; the concentration in the oil phase of PMMA or co-polymer is 1.6% w/w and concentration of all oils are 2.2% w/w. * concentration in the aqueous phase.*

In order to study the oil absorption technique,[28] 150µl of the oils perfluorooctane, perfluorodecalin, or trimethyl(pentafluoro phenyl)silane was added to 500µl of

polystyrene latex particles in small sample tubes. The mixtures were ultrasonicated for typically 1.5 hours at 30°C until all of the oil had been incorporated inside the polystyrene matrix as judged by no visual appearance of oil in the sample tubes. These swollen particles were characterized by both NMR and light scattering.

The co-polymer particles were dialyzed (Spectrum Spectra/Por® Biotech, cut-off 300 kD) against an excess of pure water (typically 10 mL suspension and 2 L H_2O during one week with fresh water each day) to remove the PVA.

Table 2: Formulation and processing conditions for the particles with absorbed oil

Sample Code	SF1	SF2	SF3	F.O	F.D
Type of Oil	F-silane	F-silane	F-silane	F-octane	F-decalin
Sonication time	1.5 h	2h	1.5h	1.5h	1.5h

F-Silane=trimethyl(pentafluorophenyl)silane; F.D=perfluorodecalin; F.O=perfluorooctane;

Several pairs of organic-aqueous phases with two different formulations were sent to Microfluidics (Microfluidics, U.S) to be processed by a microfluidizer processor under different conditions chosen by the manufacturer. The formulations differed in the molecular weight of the PMMA according to Table 3 below and the codes for the different samples processed are given in Table 4.

In the process 25 g of the oil and the aqueous phases were first mixed and then poured into the microfluidizer for processing. A processed system was immediately added to 40 g of the aqueous phase while stirring under the same conditions as using a homogenizer and the organic solvent was evaporated overnight. The interaction chamber configuration, the pressure, and the number of passes were varied during the course of the experiments to achieve the goal. The samples tested on the M-110P microfluidizer processor required a double batch (i.e. 50 g of the aqueous phase and 50 g of the oil phase) because of volume restrictions.

Table 3: Formulations for the samples sent to microfluidics

Formulation	PVA%*	PMMA%*	M_w PMMA	DCM	Acetone %	F.D%
1	2	1.6	350000	86.2	10	2.2
2	2	1.6	95000	86.2	10	2.2

*F.D=perfluorodecalin; DCM=dichloromethane; * concentration in the aqueous and in the oil phase.*

Table 4: Processing conditions of different samples prepared by microfluidizer.

Sample Code	Passes	Processor	IXC*	pressure (Psi)
8B1	10	M-110S	F20Y (75 µm)	20,000
8C1	3	M-110S	F20Y (75 µm)	10,000
2A1	3	M-110S	H30Z (200 µm)	10,000
2B1	3	M-110S	H30Z (200 µm)	5,000
3G1	10	M-110P	F12Y (75 µm), H30Z (200 µm)	30,000
3H1	15	M-110P	F12Y (75 µm), H30Z (200 µm)	30,000
4Q2	10	M-110P	F12Y (75 µm), H30Z (200 µm)	30,000
4R2	5	M-110P	F12Y (75 µm), H30Z (200 µm)	30,000
4S2	15	M-110P	F12Y (75 µm), H30Z (200 µm)	30,000
9A2	2	M-110P	L210Z (250 µm)	2,000
9B2	3	M-110P	L210Z (250 µm)	2,000
9C2	5	M-110P	L210Z (250 µm)	2,000
30A2	5	M-110P	F12Y (75 µm), H30Z (200 µm)	30,000
30B2	10	M-110P	F12Y (75 µm), H30Z (200 µm)	30,000
30C2	17	M-110P	F12Y (75 µm), H30Z (200 µm)	30,000

** IXC = Interaction chamber: a cylindrical module with a specific orifice and channel design through which fluid is conducted at high pressures to control shear rates.*

3.3 Characterization Techniques and Sample Preparation

3.3.1 DLS and SLS

Both dynamic and static light scattering (DLS and SLS, respectively) experiments were carried out with an ALV - goniometer system (ALV-CGS3, ALV-GmbH, Langen/Germany) which is connected to an ALV-Correlator. The software for Windows includes full support of the ALV- goniometer system. The angular range of the goniometer is from 17° to 150° scattering angle with a resolution of 0.025°. The instrument is equipped with a HeNe laser (22mW output power) operating at 632.8 nm. The laser needs about 1 hour warm up to stabilize before measurements. The

single photon detector transfers the pulses to the correlator to get the autocorrelation function. There is a thermal controller which controls the temperature all the time. The sample holder is thermostated decalin which has quite the same refractive index as glass. The decalin is kept in a specially made circular glass beaker of high quality quartz placed with its centre in the section point between the incoming and the scattered light. To get rid of dust and bubbles in the decalin, it was filtrated in place during typically 10 min before a measurement.

Laser, correlator, and thermal controller were switched on at the same time to start up the measurement. Pumping the decalin and positioning the sample into the sample holder were the second and third steps before starting the measurements. After each step one hour was required for temperature stabilization. The attenuator of the laser beam was set to give a counting rate of about 200 kHz. A static light scattering experiment was carried out at either 52 or 26 angles from 20° to 150° with different angular steps by changing the position of the goniometer after each measurement. For each angle 3 runs (measurements), each 30 seconds, were carried out. All these measurements were controlled by the software. DLS measurements were carried out for 5 different angles (30°, 60°, 90°, 120°, and 150°) with one run of 100 seconds at each angle. All measurements were carried out at 296 (±0.05) °K.

In this work the Contin procedure was the first choice to determine size and size distribution from the correlation function. Though, for very narrow size distributions or in some other cases when Contin showed weird results and did not work properly, the other methods (cumulants or Schultz) were used. The data from DLS were analyzed and reported as size and size distribution. The data from SLS were analyzed using two different SigmaPlot programs, one correcting for backscattering in the SLS data and the other to find the radius of gyration (R_g) and to investigate what the data said about the type of the particle (hard sphere, core-shell, or microgel particle) that was studied, as described earlier.

Sample preparation is a very crucial part of light scattering experiments. The sample should be very clean, free of dust and bubbles. Therefore, all the glasswares were cleaned carefully in four steps; first they were rinsed with a lot of tap water, then they were washed with 2% Hellmanex solution in Milli-Q water carefully, rinsed again with a lot of Milli-Q water, and finally rinsed with very clean ethanol 99%. At the end they were blown with nitrogen gas and kept into a dust free place at 25°C. The water, that the sample was supposed to be dissolved in, was degassed under reduced pressure for several times (typically 5 times) to get rid of the air and bubbles inside the water. Degassed water was filtrated through a 100 nm filter. A small volume of the particle dispersion was dispersed in the degassed filtrated water to give a weight fraction of particles typically around 10^{-5} - 10^{-6} w/w to avoid multiple scattering. The system was mixed for 90 sec, (a reference system also ultrasonicated during typically 30 sec) and filtrated again directly into the cyvette with different filters depending on the particle size. During all procedures dust and dirt were tried to be avoided.

3.3.2 NMR Diffusometry

^{19}F NMR and NMRd experiments were carried out at 298 (±0.1) K with a Bruker 600MHz spectrometer equipped with a diffusion probe with a maximum gradient of 12 Tm^{-1}. The parameters such as length of the gradient pulses, δ, the observation time

(sometimes so-called diffusion time, i.e. the time between the gradients), Δ, and the number of gradient steps were varied for different samples. The attenuated NMR signals, also called echo-decays, were normalized and evaluated using Matlab. The Stejskal-Tanner equation (Eq. 18) was finally fitted to the data.

In this work NMRd was carried out on one sample (BF10) diluted with D_2O to 9 different particle concentrations (0.05, 0.1, 0.185, 0.375, 0.625, 1.25, 2.5, 3.75, and 5 %w/w). In order to prepare the particles at these different concentrations, the particle dispersion BF10 was first concentrated by stirring the suspension in a fume hood for 3 days and after that diluted with D_2O to different percentages from the suspension with the highest concentration directly in the NMR tubes. The concentration of the concentrated BF10 dispersion was calculated from the loss of the weight, knowing the initial concentration according to the formulation protocol.

3.3.3 Quartz Crystal Microbalance with Dissipation (QCM-D)

The QCM-D experiments were carried out with a D300 machine (Q-Sense AB) with the static solution chamber at 23 °C, using a AT/cut piezoelectric quartz crystals covered with gold. Its fundamental frequency was 5 MHz. Measurements were carried out by applying an electrical field over the piezoelectric quartz crystal to cause oscillation of the crystal at its own frequency. Adsorption of polymer (PMMA) on the surface of the crystal caused a change in the oscillation frequency of the crystal. By monitoring the changes in frequency the mass uptake was calculated from the Sauerbrey equation (Eq. 19).

The Sauerbrey equation is valid for a PMMA film, which is a rigid thin film (or adsorbed layer) and the dissipation should then be constant. However, if the adsorbing polymer (PVA) forms a flexible layer on the surface (PMMA), the dissipation will change during the adsorption, and the Sauerbrey equation will not be valid. Other mathematical models must then be used, such as the Voigt model as described before, in order to interpret the data and calculate the mass uptake and consequently the thickness of the absorbed layer.

The crystals were cleaned carefully based on a crystal cleaning protocol accordingly; first the crystals were put in a UV/ ozone chamber for 10 min, after that they were immersed in a 1:1:5 mixture of H_2O_2 (Merck, 25%), NH_3 (Merck, 25%), and Milli-Q water for 5 min at 78°C. They were then rinsed with Milli-Q water and dried with nitrogen gas and put in the UV/ozone chamber for 10 more minutes. An 1% w/w PMMA solution in chloroform was used to coat the crystal using a spin coater at 2000 rpm for 60 sec. The coated crystals were kept at room temperature overnight in order to get complete evaporation of the chloroform. The adsorption of PVA was measured from solutions with 10 different concentrations (0.0001, 0.001, 0.003, 0.009, 0.027, 0.081, 0.243, 0.729, 1, and 1.2% w/w) onto the PMMA coated crystals. At the end the results were analysed using the one-layer visco-elastic model based on Voigt's spring/dashpot theory included in Q-tools software (QTools) provided by Q-Sense AB.

Desorption of the PVA was also studied by using a crystal with adsorbed PVA (adsorbed from a 0.729 %w/w solution). Pure water was used to wash the crystal several times until only small or no further changes in dissipation or frequency could be detected.

3.3.4 Scanning Electron Microscopy

A LEO Ultra 55 FEG SEM was used to prepare the SEM images. As already mentioned samples should be dry when using the SEM-technique. Therefore the microcapsule suspension was spin coated on a microscopy glass slide, and kept at room temperature overnight to dry. The glass was attached on the SEM stub carbon stick. In order to make the sample conductive the sample was coated with a thin layer of gold in a JFC/1100E sputter coater. The chamber was evacuated to a pressure of 10 Pa, and a sputtering current of 10mA was applied for 1.8 minutes to get a layer with a thickness of about 120 Å.

4 RESULTS AND DISCUSSION

In this chapter results from four different characterization methods are presented, namely light scattering, NMRd, QCM, and SEM for some different samples which each are representative of a group of the samples.

4.1 Light Scattering

Dynamic light scattering measurements were carried out on all the samples both prepared by homogenizer and microfluidizer as well as the samples prepared by oil absorption into the particles. Sizes and size distributions are shown in the following tables.

*Table 5: Results from measurements and calculation of sizes and size distributions of microcapsules prepared by rotor/stator homogenizer. The sample codes can be found in Table 1. Reported sizes are the estimated hydrodynamic diameters.**

Sample code	BF1	BF2	BF3	BF4	BF5	BF6	BF7	BF8	BF9	BF10	BF14	BF17
Size(nm)	4000	2500	432	650	480	740	800	580	308	300	800	980
Size distribution(CV)	0.39	0.36	0.3	0.38	0. 3	028	0.34	0.34	0.23	0.23	0.3	0.16

** The CV is the coefficient of variation. The result for the co-polymer particle BF14 was obtained immediately after dialysis.*

The results in Table 5 show the influence from different processing parameters. It is obvious that a decreased the PMMA molecular weight in the oil phase led to both a reduction of sizes and more narrow size distributions. Since the viscosity of a polymer solution $\eta \propto M^{3.4}$, a reduction in molecular weight was expected to result in a decreased viscosity. Lower viscosity of the oil phase could have resulted in an easier droplet break up,[11,13] which could have given a decrease in size and more narrow size distributions.

As reported above in Table 1 different shear rates had been applied to prepare the microcapsules. The results reported in Table 5 clearly show that higher shear rates resulted in smaller particles, which probably were due to the fact that more intense turbulence caused by higher shear rates might have facilitated the droplet break up,[11] and consequently could have resulted in smaller particles.

Further, according to Tables 1 and 5 increased temperatures seemed to have caused smaller particles. This could have been the result of a reduction of viscosity by increasing temperature.

Finally, the results showed that the type and concentration of the emulsifier affected the size and size distribution. The results showed that by increasing the PVA concentration, the size and size distributions decreased. However, further increase in the PVA concentration resulted in an increase in size and size distribution. The first reduction trend could have been due to two facts. First, by increasing the PVA concentration, the viscosity of the aqueous phase will increase, and the viscous forces generated by the continuous phase, would help the droplet disruption. Consequently the particles will get smaller. It will also affect the ratio in viscosity between the oil and the aqueous phase. Interestingly, by using 0.5% PVA solution emulsification was

not successful (no formed particles). Second, increasing the PVA concentration there would be enough emulsifier in the emulsion to migrate readily to the newly created surface and prevent coalescence of droplets. But the increase in particle size at high concentration was probably due to the fact that high concentration polymer emulsifiers might have depressed the turbulence, which then could have resulted in a less efficient disruption of the emulsion droplets.[11]

Table 6: Results from measurement and calculation of size and size distribution of microcapsules prepared by microfluidizer. The sample codes can be found in Table 4. Reported sizes are the estimated hydrodynamic diameters.

Sample code	8B1	8C1	2A1	2B1	3G1	3H1	4Q2	4R2	4S2	9A2	9B2	9C2	0A2	0B2	0C2
Size(nm)	280	424	480	571	308	251	377	292	261	648	428	375	253	139	119
Size distribution(PDI)	0.21	0.27	0.25	0.21	0.1	0.12	0.18	0.11	0.11	0.2	0.1	0.18	0.25	0.11	0.1
Size distribution(CV)*	0.46	0.52	0.5	0.46	0.31	0.34	0.42	0.33	0.33	0.44	0.31	0.42	0.5	0.33	0.31

** The CV is the coefficient of variation*

In Table 6 are the DLS results shown for the samples prepared by the microfluidizer technique. Two different formulation protocols were used; six samples according to formulation protocol 1, and nine samples according to formulation protocol 2 (see Table 3). The difference between these two formulation protocols was the molecular weight of PMMA. In formulation type 1 PMMA molecular weight was 350 kD and in formulation type 2 it was 95 kD. It is seen from the results in Table 6 that formulations with the higher molecular weight resulted in bigger particle size and higher polydispersity index, when compared to the ones processed under the same conditions. The explanation for this could probably be based on the same arguments as was discussed for samples prepared by homogenizer.

The results also showed that the samples prepared by microfluidizer compared to samples prepared by homogenizer had smaller particle sizes but quite the same polydispersity index ($CV = \sqrt{PDI}$). Thus, using a microfluidizer for this type of systems did not help to get a narrower polydispersity.

DLS experiments were also carried out on the latex particles with absorbed oil. The appearance of these particles is summarized in Table 7.

Table 7: Properties of particles prepared by the absorption technique.

Samples Code	SF1	SF2	SF3	OF	DF
Type of Oil	F-silane	F-silane	F-silane	F-octane	F-decalin
Sonication time	1.5h	2h	1.5h	1.5h	1.5h
Appearance	Complete Absorption	Particle aggregation	Particle aggregation	No or little absorption	Particle aggregation

The DLS result for the SF1 showed that the hydrodynamic diameter of the particles one day after preparation was 129 nm with CV=0.136. However, after one week the hydrodynamic diameter had decreased to 109 nm (close to the size of the "naked" latex particles), while the CV was essentially the same (CV=0.129). This reduction in size could have been due to the evaporation of the trimethyl(pentafluoro phenyl)silane. The same result was found in the NMRd experiment. Also, it seemed that the absorption technique was quite sensitive to the processing conditions. For example, an increased sonication time from 1.5 h to 2 h resulted in an aggregation of the particles SF2 as compared to SF1. Also, aggregation of particles was found to occur even though the sonication was the same (SF3 compared to SF1). Temperature would in this respect be very important.

Static light scattering measurement was carried out on some of the samples. For comparison, experiments were also carried out with a commercial hollow sphere (water in the core and as medium) with size = 404 nm and CV = 0.32. The result is reported in Figure 12 where the plots of $P(\theta)$ *vs.* q are shown for the experimental data and simulations of different types of particles. Although the CV was relatively high (CV=0.32 corresponds to a polydispersity index of 0.1), it is seen in Figure 14 that the only model that could be used to get coincidence with the experimental data was indeed the polydisperse hollow sphere. This hollow sphere is a special case for the more general core-shell particle. In the hollow sphere the refractive index of the core is the same as for the medium, i.e. water, while the refractive index of the shell is that for the polymer. The result clearly showed the possibilities to discriminate between different models for the analysis, i.e. between a hard sphere and a hollow sphere with different degrees of polydispersities. Further, the theory for the form-factor for the core-shell particle allows the calculation of several interesting parameters, which however not will be discussed here.

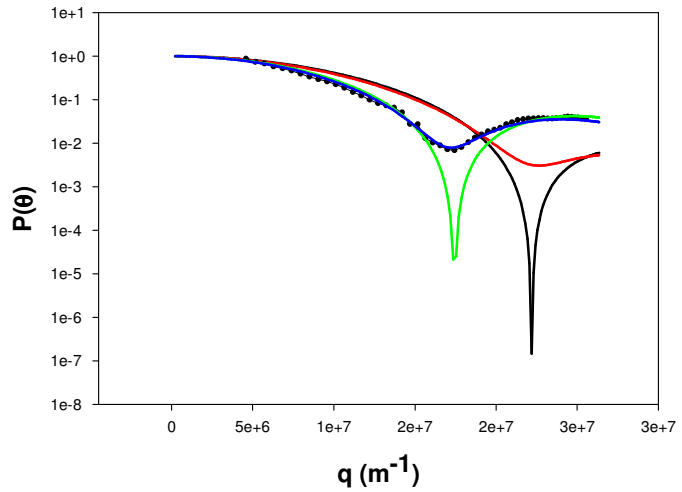

Figure 14: Plot of $P(\theta)$ vs. q for different systems. Black dots: experimental; Black curve: monodisperse hard sphere (radius = 202 nm); Green curve: monodisperse hollow sphere (outer radius 202 nm, shell thickness = 43 nm); Red curve: polydisperse hard sphere (radius = 202 nm, CV=0.32); Blue curve: polydisperse hollow sphere (radius 202 nm, shell thickness = 43 nm; CV = 0.32)

In Figure 15 the results from studies of the particle BF10 (homogenizer; size = 300 nm; CV=0.23) are shown. It was not possible to get any coincidence what so ever between the experimental data and any of the models for a hard sphere or a core-shell. The size of the particles (300 nm) would indeed have given a minimum in the experimental curve provided any of the core-shell models had been right. Instead it is seen that the experimental data were far above what they should have been. Thus, these particles could not be considered as core-shell particles.

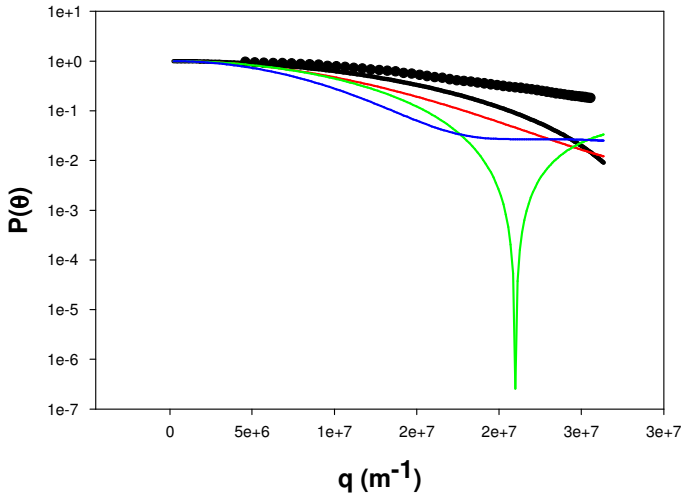

Figure 15: Plot of P(θ) vs. q for the sample BF10. Black dots: experimental; Black curve: monodisperse hard sphere (radius = 150 nm); Green curve: monodisperse hollow sphere (outer radius 150 nm,); Red curve: polydisperse hard sphere (radius = 150 nm, CV=0.23); Blue curve: polydisperse hollow sphere (radius 150 nm; CV = 0.23)

On the other hand, the much bigger particle BF17 (homogenizer; size = 980 nm; CV=0.16) clearly gave an oscillating *P(θ)* as expected for such big particles. This is shown in Figure 16. However, the agreement between the experimental and theoretical curves was again not satisfying. Increasing or decreasing the molecular weight, the size, and/or the shell thickness did not result in any better agreement. Tentatively one reason for the disagreement could have been that the more complicated Mie-theory to predict the static light scattering results was not used, simply because the difficulties to include effects from polydispersity in such calculations. The major reason, however, was probably that the core-shell model used was not adequate.

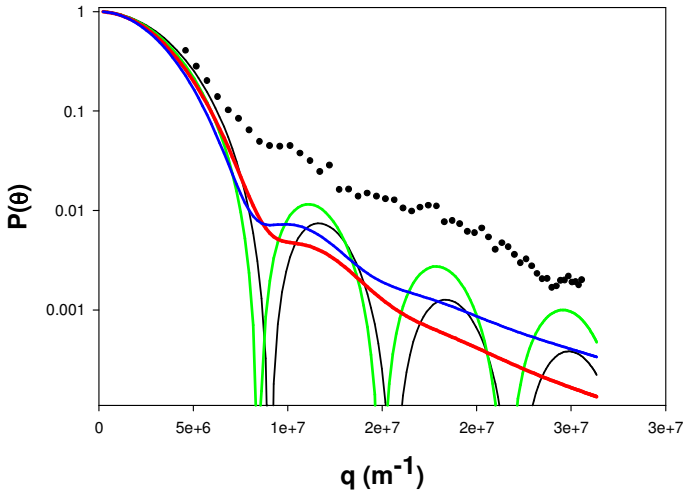

Figure 16: Plot of P(θ) vs. q for the sample BF17. . Black dots: experimental; Black curve: monodisperse hard sphere (radius = 490 nm); Green curve: monodisperse hollow sphere (outer radius 490nm,); Red curve: polydisperse hard sphere (radius = 490 nm, CV=0.16); Blue curve: polydisperse hollow sphere (radius 490 nm; CV = 0.16)

The results for one of the particles made with microfluidizer, 3G1 (size=308 nm; CV=0.31) are shown in Figure 17. Due to the size and the CV of this particle an obvious minimum should have been detectable. However, as for the BF10 particle (Figure 13) the experimental data again was much higher than any of the theoretical models used and no minimum could be seen.

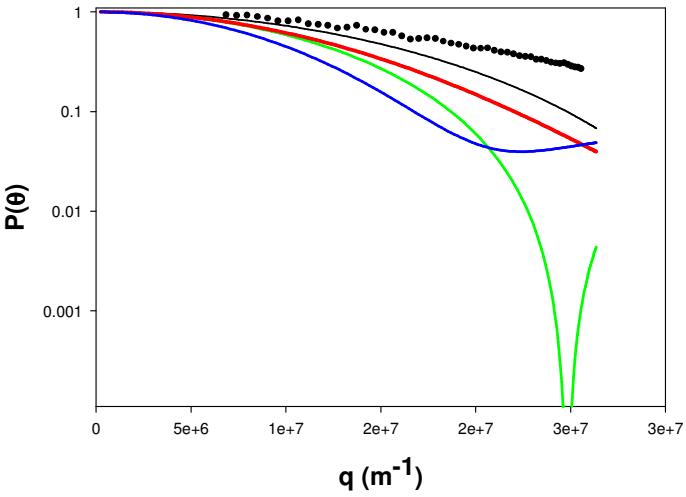

Figure 17: Plot of P(θ) vs. q for the sample for 3G1. Black dots: experimental; Black curve: monodisperse hard sphere (radius = 154 nm); Green curve: monodisperse hollow sphere (outer radius 154nm,); Red curve: polydisperse hard sphere (radius = 154 nm, CV=0.31); Blue curve: polydisperse hollow sphere (radius 154 nm; CV = 0.31)

The results presented for the BF10, BF17, and 3G1 particles thus clearly showed that these particles could not be regarded as (classical) core-shell systems, i.e. as particles with a well defined core surrounded by a well defined shell. An alternative would perhaps be to visualize them as "microgel particles". Such particles have been discussed in papers in connection with light scattering experiments. Unfortunately no closed equations for $P(\theta)$ have been presented for polydisperse microgel particles, but only the monodisperse case with some assumptions regarding the distribution of the core material in the particles. Thus, in the paper by Fernandez-Nieves et al.[29] the particle form factor is simplified to cover only the region Rq<<1, where R is an apparent radius and q is the q-vector. The particle is composed of a core with continuously changing refractive index towards the shell. In order to apply the thoughts forwarded in other papers, it is necessary to carry out a complicated numerical integration, which not was possible for the present Thesis work.

Nevertheless, the approach taken by Fernandez-Nieves et al.[29] is presented in Figure 18 together with the experimental studies of system BF10. It is seen that the agreement between the experimental and simulated $P(\theta)$ was better than when using a classical core-shell particle model. The disagreement at higher q-values was expected and was inherent in the theoretical model used. However, the results gave some indications that the present particles probably more should be discussed assuming a concentration gradient of the oil from the centre of an apparent core out to, and perhaps even into, the shell. An even more realistic model for the present particles would perhaps be to view them as particles with a thick layer hydrated PVA chains around. This will be discussed in more detail in section 4.2.

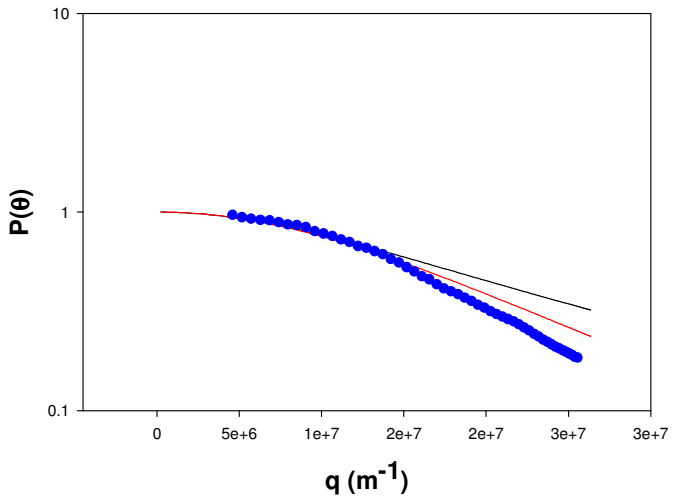

Figure 18: Plot of $P(\theta)$ vs. q for the sample for 3BF10. Black dots: experimental; Blue curve: simulated $P(\theta)$based on relation 1 discussed by Fernandez et al.[30] Red curve : simulated $P(\theta)$based on relation 2 discussed by Fernandez et al.

Finally, no reliable results could be obtained with DLS and SLS for the particles made by the co-polymer approach. These particles contained a low amount of charge on their surface to avoid the presence of extra stabilizer like PVA. However, it was found that the particle stock suspension aggregated after some days, probably due to poor charge stabilization.

All these results showed that it was not possible to describe the particles as classical core-shell systems with the proposed form factor of Eq. 11. Some support for this conclusion is found in the literature. Thus, similar systems have been studied with scanning and transmission electron microscopy by Moinard-Chécot et al.,[13] who emphasize that it is not easy to obtain direct experimental evidence of the core-shell morphology. In that paper it is said that due to the small size of particle the shell thickness is also very thin, and the particles can then not stand the sampling process for electron microscopy techniques. Moreover, they argue that the magnitude of the adsorbed PVA layer on the surface of the particle is quite the same as the thickness of the shell so it is very difficult to distinguish between the shell and the PVA layer. The thickness of the PVA layer will be discussed more in detail in connection with the QCM-D results below.

4.2 Quartz Crystal Microbalance with Dissipation Monitoring (QCM-D)

The QCM-D measurements were carried out in order to investigate the amount of PVA adsorbed on the PMMA spin coated surfaces as described in 3.3.3. Figure 19 shows the changes in frequency and in dissipation at three different overtones (3th, 5th, 7th) upon the addition of PVA with increasing concentration (from 0.0001% to 1.2%w/w.). In order to interpret the data, the graphs ΔF &ΔD vs. time (where ΔF and ΔD stand for changes in frequency and dissipation, respectively) have been divided in three regions which are depicted in Figure 17. In region I, the addition of the first concentration gave overlapping signals for both frequency and dissipation. It also shows a slight increase in dissipation. It could be concluded that the first region corresponded to a solid or rigid film adsorption.

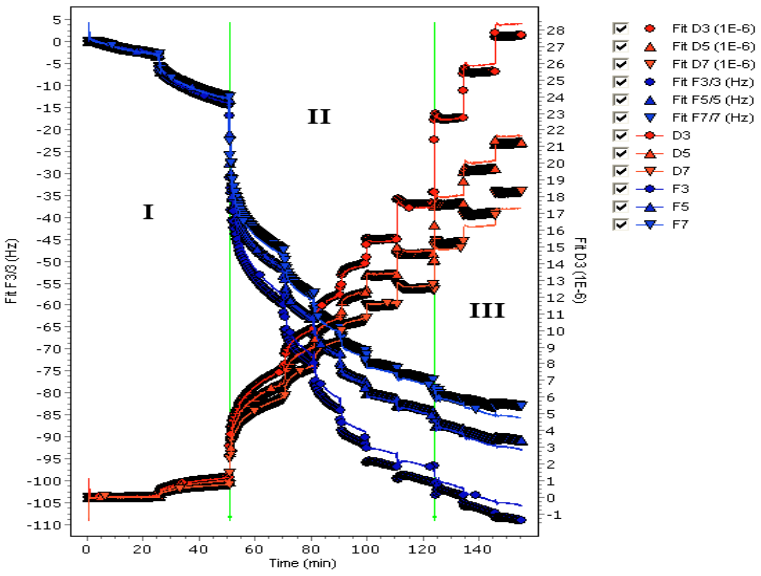

Figure 19: Blue curves= frequency vs time. Red curves= dissipation vs. time. Black curves = the Voigt model fit for both frequency and dissipation.

The second region in the ΔF &ΔD vs. time graph resulted from the addition of the six next concentrations of the PVA solution. As is clear in the graph, the responses in normalized frequency and in dissipation at the different overtones were different. Moreover, the steady state was not reached rapidly, indicating a slow kinetics of adsorption. The third region corresponds to the three last additions of the PVA solution. It can be seen that the variation of frequency and dissipation corresponding to the different overtones did not overlap. Furthermore, by addition of the 8th concentration (0.729% w/w) at 125 min, a jump in ΔD was observed while the ΔF did not change much. This could be due to either a bulk effect or reorganization of the polymer on the surface. The bulk effect could be expected due to the viscosity of the bulk solution close to the surface.

In Figure 20 the ΔD vs. ΔF plots are shown for the three overtones. It is seen that in region I the linear change in D was small when decreasing the frequency. This was in agreement with the discussion in connection with Figure 19. The data in region II showed the typical behavior expected if a soft surface was building up, with no or small differences between the different overtones. Again this was in agreement with the discussion concerning the results in Figure 19. Finally, at the start of region III (addition of the 8th concentration) the overtone curves were split and the slopes changed. These results could have been due to either the bulk effect or reorganization of the polymer on the surface. It was again in a good agreement with the results from the previous graph.

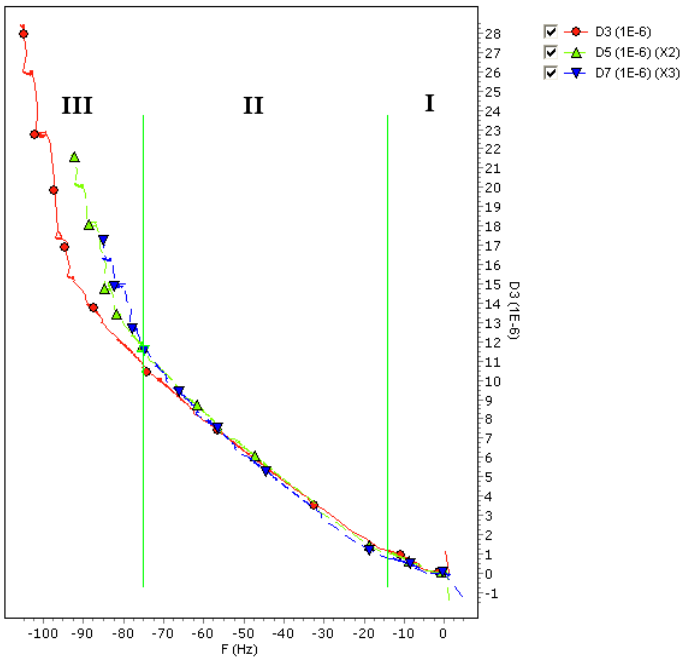

Figure 20: ΔD vs. ΔF for the three overtones

The graph ΔD vs. ΔF clearly showed that the adsorbed layer on the PMMA surface was a viscoelastic layer. Thus the Sauerbrey equation (Eq. 19) was not valid here to calculate the adsorbed mass as described in section 2.6. Therefore, above a certain concentration, in order to obtain the thickness and correspondingly the mass of the adsorbed layer, the Voigt model (Eq. 21) was applied. Figure 19 also shows that the

Voigt model fitted the experimental data very well. The thickness calculated with the Voigt model at different concentrations is shown in Figure 21 as a function of time.

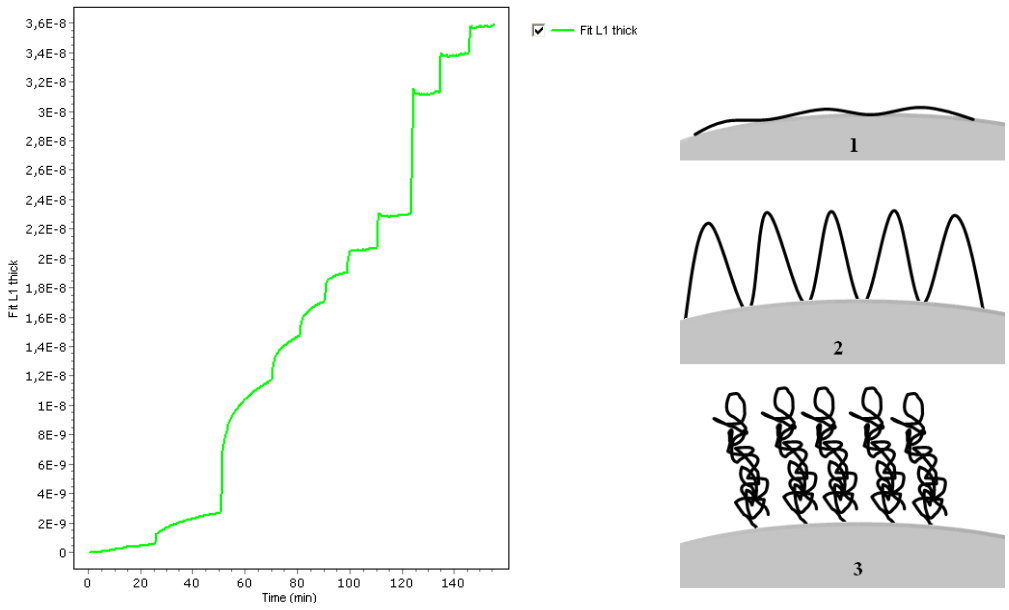

a) b)

Figure 21: a) Thickness of the adsorbed layer (m) vs. time (min). b) Schematic illustration of polymer conformation in the three regions (I to III from top to bottom)

The increase of the concentration led to a growth of the thickness of the film. In region I the increase of the thickness was very small (about one nm), which could have been due to so-called solid adsorption as mentioned before. Thus, for these low concentrations added, the adsorbed polymer chains would have a flat conformation on the surface as depicted in Figure 21bI. The second region of the graph showed that by increasing the concentration, the thickness was increased and the first jump in the thickness was most likely due to the fact that the concentration was ten times more than in the previously added solution. One could then imagine that the polymer chains adsorbed to the surface in this region as exhibited in Figure21bII. Finally, the sudden increase in the thickness in region III was either due to the bulk effect or to the reorganization of the polymer chains on the surface. One result could be that the chains were packed closely and were standing on the surface as depicted in the Figure 21bIII.

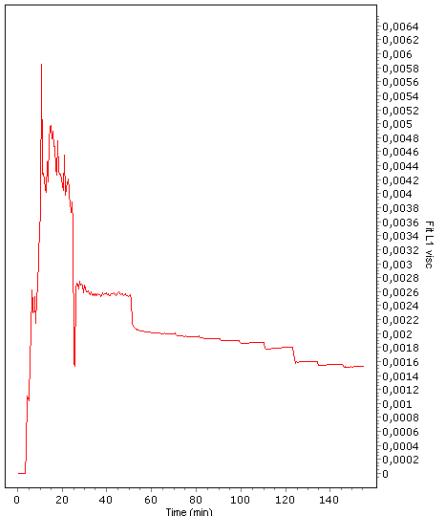

Figure 22: The plot of viscosity of the adsorbed layer vs. time

This interpretation was correlated to the values of the viscosity estimated in the modelling. The viscosity (kg $m^{-1}s^{-1}$) vs. time (min) extracted from the Voigt model is shown in Figure 22. The changes in viscosity during time (by changing concentration) agreed with the interpretation of the changes in thickness. In the first region of this graph the viscosity was very high which could be due to the solid adsorption and the noise was due to the fact that the Voigt model was not very suitable to describe rigid films. Furthermore, the other two regions were in agreement with the other results. Finally, the thickness of the adsorbed PVA was also plotted versus concentration on a logarithmic scale and is shown in Figure 23.

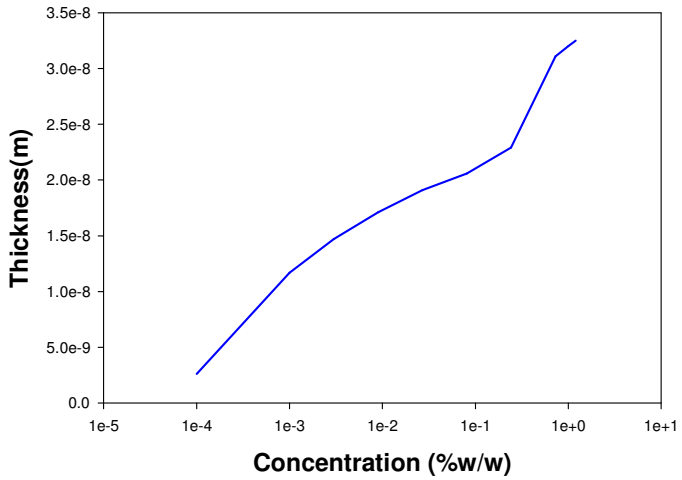

Figure 23: Thickness of adsorbed layer of PVA vs. concentration of PVA

It is seen that after the 8th addition (c = 0.729% w/w) a sudden increase in the thickness could be noticed. However, after this increase, the thickness reached almost

a plateau value of about 32 nm. This could then be considered to occur at the highest amount of PVA that could adsorb on the PMMA surface. An approximate amount of adsorbed PVA could then be calculated to 3840 ng/cm^2 from the density of 1200 kg/m^3 accordingly:

$$\rho = m/v \longrightarrow \frac{1200kg}{1m^3} = \frac{x}{1m^2 \cdot 3.2 \cdot 10^{-8} m} \longrightarrow x = 3840 \times 10^{-8} kg\ m^{-2} = 3840\ ng\ cm^{-2}$$

where ρ, m, and v are the density, mass and the volume, respectively.

If we assume that all the PMMA and all the oil in the formulation make one big core-shell particle, its density, volume (V_{ap}), and surface area (A) can be calculated as follows:

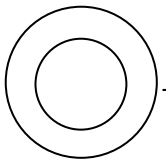

ρ_{PMMA}=1.188 g.cm^{-3} $\quad$ ρ_{Oil}=1.766 g.cm^{-3}

m_{PMMA}=1.28 gr $\quad$ m_{Oil}=1.79 g

$\rho_{total} = \omega_{PMMA} * \rho_{PMMA} + \omega_{Oil} * \rho_{Oil} \longrightarrow \rho_{total} = 1.525$ g.cm^{-3}

where ω_{PMMA} is the weight fraction of the PMMA and ω_{Oil} is the weight fraction of the oil.

$$\rho = m/v \longrightarrow 1.525 = 3.07/v \longrightarrow V_{ap} = 2.01 cm^{-3}$$

$$V = \frac{4}{3}\pi r^3 \longrightarrow r = 0.78 cm$$

The surface area of the assumed particle is:

$$A = 4\pi r^2 \longrightarrow A = 7.6 cm^2$$

Considering now, the BF10 particles, with diameter = 300 nm and assuming a monodisperse particle size distribution, the total area available for adsorption can be calculated to 601938 cm^2 accordingly:

Volume of the monodisperse BF10:

$$V = \frac{4}{3}\pi r^3 \longrightarrow V_{mBF10} = 14.13 \times 10^{-15} cm^3$$

$$\frac{V_{ap}}{V_{mBF10}} = \frac{2.01}{14.13 \times 10^{-15}} = 0.142 \times 10^{15}$$ Number of Particles in the suspension

$$A = 4\pi r^2 \longrightarrow A = 42.39 \times 10^{-10} cm^2$$ Surface area of one particle

$$A_{total} = 142 \times 42.39 \times 10^2 = 601938 cm^2$$ Surface area of all particles

From the adsorbed amount and the total surface area one could calculate the amount of PVA that adsorbed on the PMMA surface as follows:

$$\frac{1cm^2}{3840ng} = \frac{601938cm^2}{x} \longrightarrow x = 2311442000\ ng = 2.31\ g$$

Therefore, 2.31 g of PVA was needed for the suspension with the formulation used in this work (4g PVA) which means that around 57.5% of the PVA adsorbed on the surface of the particles in the stock suspension.

A second type of QCM-D experiment was also carried out. A PMMA coated crystal with adsorbed PVA was washed with pure water to follow the desorption of the PVA from the surface. The results are presented in Figures 24a and b.

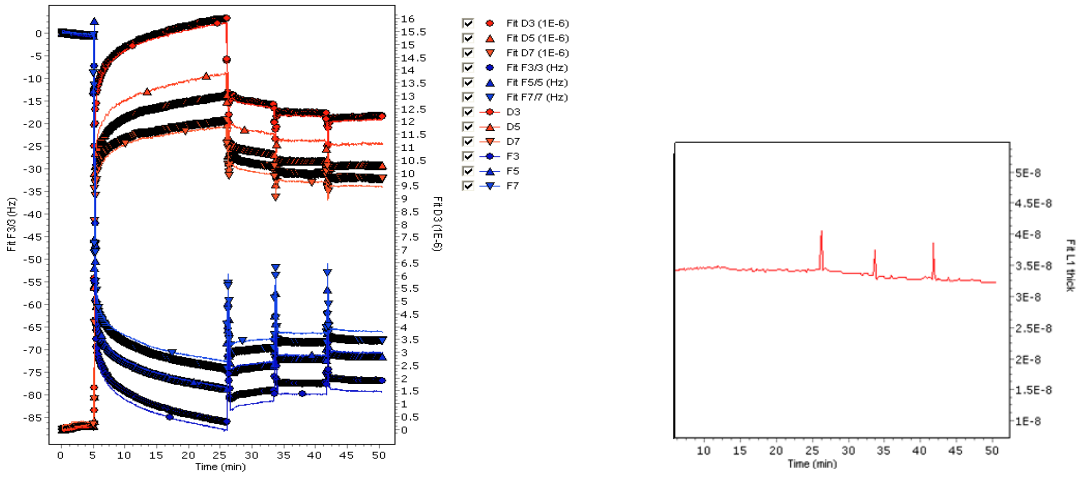

a) b)

Figure 24: a) *Blue curves= frequency vs time. Red curves= dissipation vs. time. Black curves = the Voigt model fit for both frequency and dissipation. b) Estimated thickness (m) of adsorbed layer according to the Voigt model.*

It is seen that, surprisingly, only minor changes in the dissipation, frequency and thickness could be found even after three consecutive washings with water. The results indicated that the PVA might have been more or less irreversibly adsorbed to the PMMA surface, which then had consequences for how the LS results had to be interpreted.

Thus, if the amount (57.5%) of adsorbed PVA onto the PMMA surface of the particles had adsorbed irreversibly, the dilution of the particle suspension for the light scattering experiments would have given a system with particles with a thick layer of PVA on the surface. Indeed, irreversible binding of PVA to PMMA has been proposed to be possible by Zhang et al.,[31] but no explanation was given in that paper for the mechanism. For such a system the particle form factor $P(\theta)$ should then have been simulated with a more complicated model, containing the oil core with refractive index n_C, a shell with refractive index n_S, and an adsorbed PVA layer with refractive index n_P in a medium with refractive index n_m. Moreover, the thickness of the

adsorbed layer in such a model has perhaps to be of similar thickness as the shell itself or thicker. So far no such model for $P(\theta)$ has been presented in literature.

On the other hand, it can be argued that the PVA can not be bound irreversibly on the surface due to an established equilibrium between the adsorbed PVA and PVA in the bulk. Thus, when such a particle stock suspension is diluted to make light scattering experiments possible with no multiple scattering in the data, the adsorbed amount of the PVA would decrease, leaving only a thin layer of adsorbed PVA on the surface and very low concentrations in the bulk. Neither the thin adsorbed PVA layer, nor the PVA in the bulk, would then be detectable in the light scattering experiments. For such a situation the form factor used would have been correct and the conclusion is that the system studied was not a classical core-shell system. In light of the QCM-D desorption results, it is nevertheless tempting to believe that the PVA was bound irreversibly to the particle PMMA surface, a phenomenon which, however, requires a more detailed understanding to be fully acceptable.

4.3 Nuclear Magnetic Resonance Diffusometry

The ^{19}FNMR clearly gave peaks that showed that the fluorinated oils were in their liquid state. ^{19}F NMR spectra for pure perfluorooctane and the encapsulated perfluorooctane are shown in Figure 25.

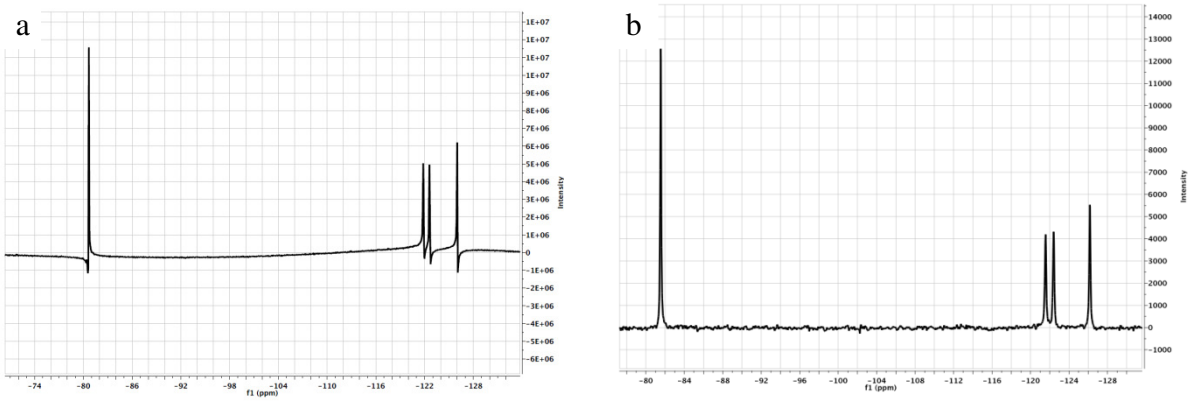

Figure 25: ^{19}F NMR spectra for (a) pure perfluorooctane and (b) the encapsulated perfluorooctane.

NMRd measurements were then carried out on both fluorinated oil particles and F-silane absorbed particles. The measurements on the F-silane absorbed particles showed that the signals from the oil disappeared after one week, which could have been due to evaporation of the oil during standing. This result was in agreement with the LS results. Experiments with the sample BF10, as prepared at 9 different particle concentrations as described in section 3.3.2, gave strange results The diffusion coefficients of the particles for different concentrations were determined from the slopes of the plots of intensity vs. k factor (Eq. 18). Figure 26 shows the normalized signal intensity vs k factor for the sample with the concentration 0.375 %w/w particles. Similar results were obtained for the other particle concentrations except for two of the experiments. For these, the normalized intensity (on a log scale) was neither acceptably linear nor smoothly curved, but disturbances were clearly visible.

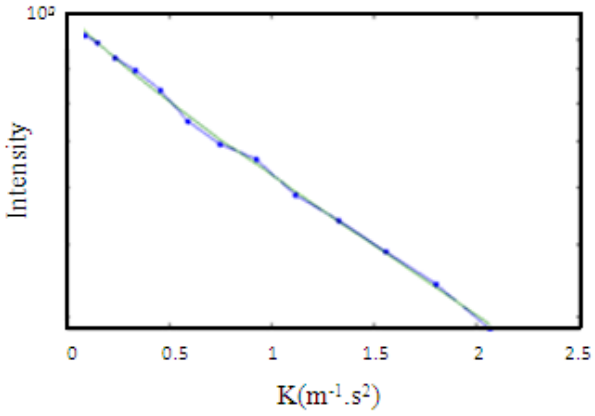

Figure 26: Normalized intensity vs k factor for the sample with the concentration 0.375 % w/w particles.

Finally, in Figure 27 the estimated diffusion coefficients of the particles are plotted vs particle concentration. The diffusion coefficients that probably were wrong, as discussed above, have been marked with an X.

It is seen that there was a slight trend in the data with decreasing diffusion coefficient upon increasing particle concentration. However, the diffusion coefficient ($6.2*10^{-13}$ m^2 sec^{-1}) at the lowest concentration was a factor 2.7 lower than the one found in the LS experiments (R_h = 150 nm, $D=1.6*10^{-12}$ m^2 sec^{-1}) when corrected for different experimental temperatures and viscosities. The expected ratio (from differences in viscosities) should have been 1.3. From each diffusion coefficient a hydrodynamic radius was calculated according to Eq. 2. The viscosity needed for the medium was calculated from published data of the specific viscosity for PVA in water,[32] and assuming that around 60% of the PVA adsorbed irreversibly on the surface of the particles for all the systems obtained from the concentrated BF10 suspension by dilution with D_2O. The results are summarized in Table 8. The results are presently not understood.

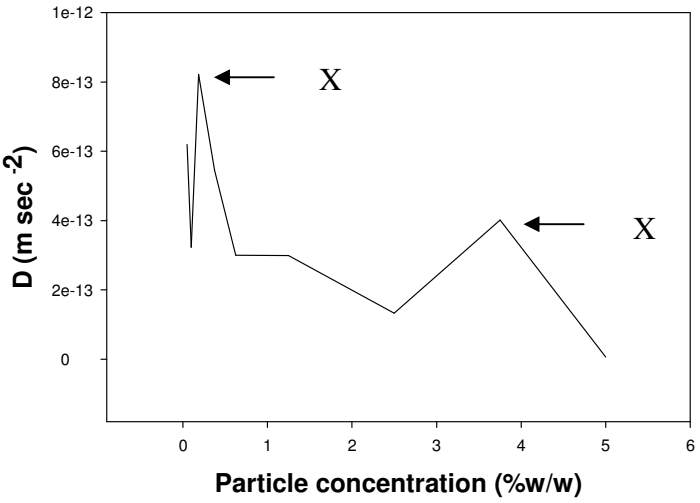

Figure 27: Diffusion coefficient vs. concentration for the sample BF10 from NMRd experiments.

Table 8: Diffusion coefficients (D) and hydrodynamic radii (R_h) obtained from NMRd experiments. The results marked X were obtained from the probably wrong diffusion coefficients discussed above.

C (%w/w)	0.05	0.1	0.185^X	0.375	0.625	1.25	2.5	3.75^X	5
$\eta*10^3$ (Pa s)	1.023	1.045	1.085	1.180	1.315	1.705	2.708	4.01	5.61
$D*10^{13}$ ($m\ s^{-2}$)	6.199	3.228	8.264	5.45	3	2.99	1.33	4.02	6.635^*
R_h (nm)	344	646	244	339	553	428	606	135	5865

4.4 Scanning Electron Microscopy

The morphology of the microcapsules was observed by scanning electron microscopy. The SEM images from three samples BF10, BF14, and BF17 are shown in Figure 25.

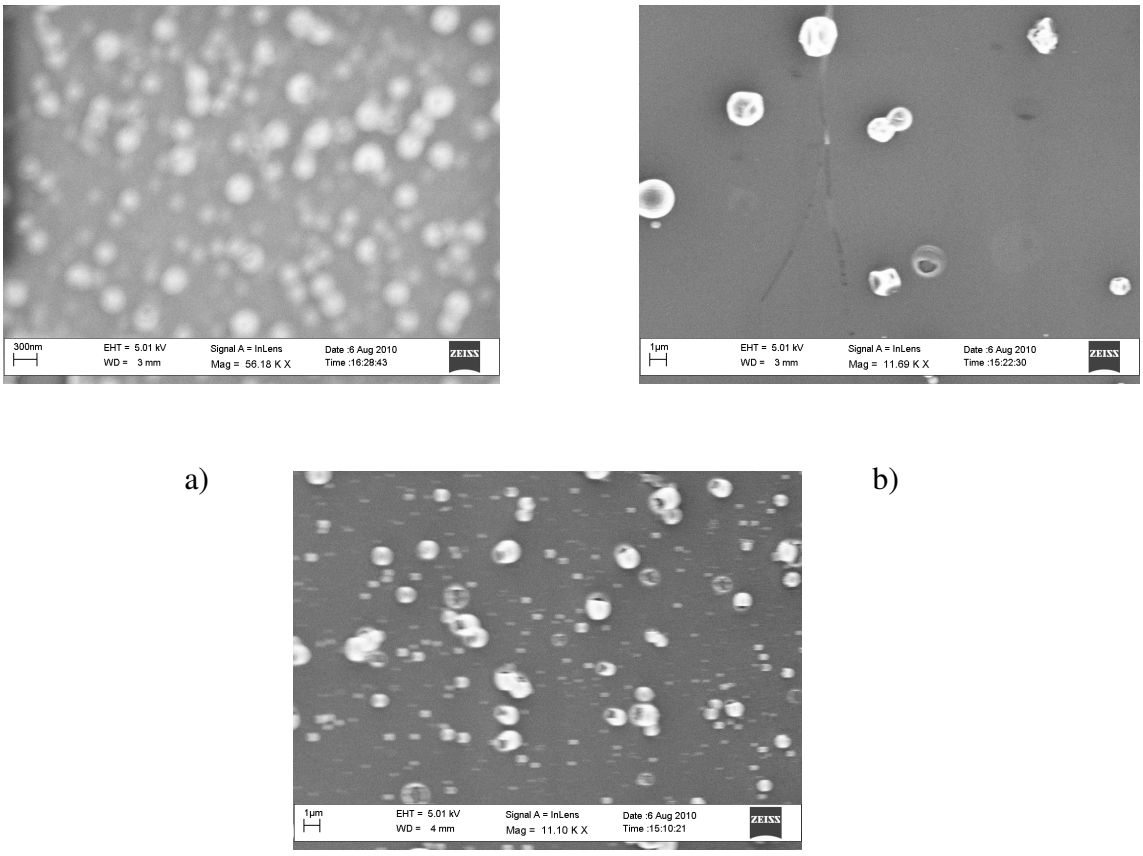

Figure 27: SEM micrographs from different suspensions; a) BF10, b) BF14 and c) BF17. The scale bars can be seen at the bottom of the images; a) 300 nm; b) and c) 1 µm.

The microcapsules were spherical and the particle size, determined from SEM micrographs, was in a good agreement with the DLS results. However, this cannot be clearly seen in Figure 25 a) due to focus problem during imaging. From the SEM micrographs it was clear that the particles were polydisperse, but practically it was not possible to determine the polydispersity since thousands of images would have been needed.

Some of the capsules in Figure 25 c) were deformed while in the other two images they were intact. This could have been due to using different types of oil in preparing the particles.

5 CONCLUSION AND FUTURE WORK

The idea behind this work was to achieve a kind of probe particles that could be detected by both NMR and light scattering. Core-shell particles with fluorinated oil as the core were chosen.

Fluorinated oil particles in different sizes from about 300 nm to 1 μm in diameter were prepared using two different techniques for emulsification (homogenizer and microfluidizer). For easily interpretable results it was intended to get particles with a rather narrow size distribution.

Both SLS and DLS were used to characterize the obtained particles. The lowest polydispersity obtained gave a relative standard deviation (CV) of the size distribution of CV=0.16, which was acceptable. However, the SLS experiments could not verify the formed particles as classical core-shell particles. The theoretical and experimental form factors did not agree.

On the other hand, QCM-D results showed that approximately 60% of the PVA adsorbed on the surface of the particles (PMMA), creating an extra layer or shell on (around) the particles. It is conceivable that if such a PVA layer is irreversibly adsorbed, the particles should best be described as core-shell particles with a thick adsorbed layer of PVA. Unfortunately no theoretical form exists for the particle form factor that could be used to interpret the SLS data. The use of scattering techniques based on X-rays or neutrons might be helpful to see the different layers and the core in such particles. An interesting future work valuable for LS applications would perhaps be to formulate a theoretical particle form factor for the present systems.

^{19}FNMR and NMRd experiments were carried out on a particle system at different particle concentrations. Despite some uncertainties concerning the NMRd experiments, a trend could be seen in the results: with higher particle concentration the diffusion coefficient decreased (and the hydrodynamic radius increased). However, the obtained diffusion coefficient at the lowest concentration was lower with a factor of 2.1 than the one found in the LS experiments. This result was not understood, since LS should in principle be more sensitive to bigger species than NMRd. However, the spectra from the ^{19}FNMR experiments clearly showed that the fluorinated oils were in their liquid state, and then most probably associated with the particles in the core.

The SEM results verified that the obtained particles indeed were in the same size range as determined with DLS.

For future work with similar particle systems it is proposed that the formulation protocols are carefully investigated. Thus, higher speed of the homogenizer, better temperature control during processing, other types of shell polymers, other compositions, etc. might help to produce smaller particles with lower polydispersity in size. Also, interactions between the core oils and the shell polymers should be investigated in more detail. An interesting approach would be to try to produce core-shell particles with a charged surface to eliminate the need for an extra stabilizer. Although this approach was tried in the present work, the particles were not stable but aggregated upon standing. However, another choice of charged polymer might give better results.

6 REFERENCES

1. M. Li, O. Rouad, and D Poncelet *International Journal of Pharmaceutics* **2008**, 363, 26.
2. G. Sorensen, A.L. Nielsen, M. Moller-Pedersen, S. Poulsen, H. Nissen, M. Poulsen, and S.D. Nygaard *Organic Coating* **2010**, 68, 299
3. M. Song. N. Li, S. Sun, and M.M. de Villiers *Pharmazie* **2005**, 60, 278.
4. C.A. Finch and R. Bodmeier *Microencapsulation*, Wiley-VHC Verlag GmbH&Co, **2002**
5. R. Bodmeier and J.W. McGinity *International Journal of Pharmaceutics* **1988**, 43, 179.
6. C.E. Mora-Huertas, H.Fessi, and A. Elaissari *International Journal of Pharmaceutics* **2010**, 385, 113
7. T. Panagiotou, S.V.Mesite. J.M. Bernard, K.J. Chomistek, and J. Fisher *Personal communication, Microfluidics Corporation 2010.*
8. World Wide Webb: Kinematica.com.ua.
9. S. Desgoulles, C. Vauthier, D. Bazile, J. Vacus, J.L. Grossiord, M. Veillard, and P. Couvreur *Langmuir* **2003**, 19, 9504.
10. P.J. Dowding, R. Atkin, B. Vincent, and P. Bouillot *Langmuir* **2004**, 20, 11374.
11. P. Becher *Encyclopedia of emulsion technology. Vol. 1, Basic theory.* Marcel Dekker, NY 1983
12. E. Pasani, E. Fattal, J. Paris, C. Ringard, V. Rosilio, and N. Tsapis *Journal of Colloid and Interface Science* **2008**, 326, 66.
13. D. Moinard-Chécot, Y. Chevalier, S. Briançon, L. Beney, and H. Fessi *Journal of Colloid and Interface Science* **2008**, 317, 458.
14. P.J. Flory *Principle of Polymer Chemistry.* Cornell University Press, Lthaca, NY 1953.
15. H. Tompa *Polymer Solutions.* Butterworths, London 1956.
16. J.Y. Lai, S.F. Lin, F.C. Lin, and D.M. Wang *Journal of Polymer Science, Part B: Polymer Physics* **1998**, 36, 607.
17. A. Loxley and B. Vincent *Journal of Colloid and Interface Science* **1998**, 208, 49.
18. A. Einstein *Annalen der Physik* **1905**, 17, 549.
19. P. Bartelemy, J. Bertolotti, and D.S. Wiersma *Nature* 2008. 453, 495.
20. W. Brown (Ed.) *Light scattering - Principle and development.* ClarendonPress, Oxford **1996**.
21. W. Burchard *Physical techniques for the study of food biopolymer.* Chapman &Hall, Glasgow, 1994.
22. L. Livsey and R.H. Ottewill *Advances in Colloid and Interface Science* **1991**, 36, 173.

23. W. Brown (Ed.) *Dynamic Light scattering*, Clarendon Press, Oxford **1996**.

24. E.O.Stejskal and J.E. Tanner. *Journal of Chemical Physics* **1965**, 42, 288.

25. B.D. Vogt, E.K. Lin, W.I. Wu, and C.C. White *Journal of Physical Chemistry B* **2004**, 108, 12685

26. World Wide Webb: www.qsense.com.

27. L.E. Nielssen and R.F. Landel *Mechanical properties of polymer and composites.* Marcel Dekker, NY 1994.

28. S. Palit and A. Yethiraj *Langmuir* **2008**, 24, 3747.

29. A. Fernàndez-Nieves, F.J. de las Nieves and A. Fernàndez-Barbero *Journal of Chemical Physics* **2004**, 120, 374.

30. I.E. Lămătic, M. Bercea, and S. Morariu *Revue Roumaine de Chimie* **2009**, 54, 981.

31. Y. Zhang, G. Ping, N. Kaji, M. Tokeshi, and Y. Baba *Electrophoresis* **2007**, 28, 3308.

32. M. Rubinstein and R.H. Colby *Polymer physics.* Oxford University Press, **2003**.

7 ACKNOWLEGMENTS

I am most grateful to my supervisors, Prof. Magnus Nydén and Prof. Jan-Erik Löfroth. They are more than supervisor to me; Magnus teaches me how to think far and Jan-Erik shows me how to build up the path to reach the far. I feel so lucky. My especial thank to Jan-Erik for his great help in the writing of my thesis. I also wish to thank Prof. Krister Holmberg for examining the work.

I am thankful to Romain Bordes for all the valuable discussions we had on my project, for all the kind help he gave with QCM experiment and for all the brilliant comments he made on the results.

Thanks to Alberta, my kind roommate, for being so patient, for listening to my explanations concerning my project and also for her practical help with figure editing. I would like to show my appreciation to Diana, Lars and Åsa for their great assistance with NMR experiment, Mariam, Maria, and Ali for their helps.

I also wish to remember Dazheng and Chlor, my former roommates in the master student room, who made the work more fun. Thanks to Ann Jakobsson and all the people at the Division of Applied Chemistry who created a very friendly environment.

I would like to show my gratitude to my patient parents and my sisters who have inspired me all my life.

Finally I wish to express my deep thanks to my dearest husband who is my best full time friend and understands all my feelings, stresses, excitements and enthusiasms; he is the most perceptive man ever. He is always ready to listen to me talking about my project and he tries to understand. He is wonderful. See, I am really really lucky.